PHYSICAL REVIEW D **90,** 034005 (2014)

Flavor structure of the unpolarized and longitudinally polarized sea-quark distributions in the nucleon

M. Wakamatsu*

Department of Physics, Faculty of Science, Osaka University, Toyonaka, Osaka 560-0043, Japan

(Received 26 May 2014; published 6 August 2014)

It is now widely recognized that a key to unraveling the nonperturbative chiral dynamics of QCD hidden in the deep-inelastic-scattering observables is the flavor structure of sea-quark distributions in the nucleon. We analyze the flavor structure of the nucleon sea in both the unpolarized and longitudinally polarized parton distribution functions within the flavor SU(3) chiral quark-soliton model, which contains only one adjustable parameter, Δm_s, the effective mass difference between the strange and nonstrange quarks. Particular attention is paid to a nontrivial correlation between the flavor asymmetry of the unpolarized and longitudinally polarized sea-quark distributions and also to a possible particle-antiparticle asymmetry of the strange-quark distributions in the nucleon. We also investigate the charge-symmetry-violation effects in the parton distribution functions exactly within the same theoretical framework, which is expected to provide us with valuable information on the relative importance of the asymmetry of the strange and antistrange distributions and the charge-symmetry-violation effects in the valence-quark distributions inside the nucleon in the resolution scenario of the so-called NuTeV anomaly in the extraction of the Weinberg angle.

DOI: 10.1103/PhysRevD.90.034005 PACS numbers: 12.39.-x, 12.38.-t, 12.38.Aw, 14.20.Dh

I. INTRODUCTION

The physics of the nucleon structure function is founded on a fine balance between perturbative and nonperturbative QCD. The standard approach to deep-inelastic-scattering (DIS) physics is based on the so-called factorization theorem, which states that the DIS scattering cross section is factorized into two parts, i.e., the hard part—which is tractable within the framework of perturbative QCD—and the soft part containing the information of the nonperturbative nucleon structure [1–5]. Customarily, the soft part is treated as a black box, which should be determined through experiments. This is certainly a reasonable strategy. We, however, believe that—even if this part is completely fixed by experiments—one would still want to know why these parton distribution functions (PDFs) take the forms so determined. Furthermore, we now realize that a key ingredient to revealing the nonperturbative chiral dynamics of QCD is hidden in the soft part of the DIS physics in the form of the flavor structure (or flavor dependence) of the sea-quark (or antiquark) distributions [6–17]. Unfortunately, what can be extracted from the well-founded inclusive DIS analyses are only the combinations of quark plus sea-quark (or antiquark) distributions. To separate out antiquark distributions, we need either neutrino-induced DIS scattering measurements, semi-inclusive DIS (SIDIS) measurements, or Drell-Yan measurements. Because of the smallness of the neutrino-induced DIS cross section, here we are forced to use nuclear targets, which inevitably introduces large theoretical uncertainties in addition to statistical errors arising from the smallness of the event-counting rate of neutrino-induced reactions [18–24]. On the other hand, a lot of efforts have been made towards understanding the SIDIS mechanism [25–29], in particular the fragmentation mechanism of a quark or an antiquark into observed hadrons [30–35]. Still, one must say that our understanding of the semi-inclusive reaction mechanism remains at a fairly lower level than that of inclusive reactions. A complementary approach to DIS physics is necessary here to clarify the possibly important role of the chiral dynamics of QCD in the DIS physics, based on effective models of QCD or lattice QCD.

Although there are lots of models of baryons, the chiral quark-soliton model (CQSM), first proposed by Diakonov, Petrov, and Pobylitsa, would probably be the best one [36], at least as an effective model of the internal partonic structure of the baryons including the nucleon. (The practical numerical method for handling the CQSM was established in Ref. [37] based on the general methodology of Kahana and Ripka [38]. The unique feature of the CQSM, which plays an important role in the so-called nucleon spin problem, was also pointed out in this paper. For early reviews of the CQSM, see Refs. [39–42].) The CQSM has a lot of merits over other effective models of baryons. First, it is a relativistic mean-field theory of quarks, with the inclusion of infinitely many Dirac-sea orbitals, which means that it is a field-theoretical model including infinitely many dynamical degrees of freedom. Second, the mean-field is of hedgehog shape, in harmony with the nonperturbative dynamics expected from large-N_c QCD. One interesting consequence of this unique feature of the model is the strong spin-isospin correlation (or anti-correlation) in the generated nucleon seas [37]. Third, in

*wakamatu@phys.sci.osaka-u.ac.jp

 © 2014 American Physical Society

association with the first advantage, its field-theoretical nature enables us to make a reasonable estimation of not only quark distributions but also of antiquark distributions [43–53]. Last but not least, only one parameter of the flavor SU(2) version of the model, i.e., the dynamically generated quark mass M, is already fixed to be $M \simeq 375$ MeV from low-energy phenomenology as well as on theoretical grounds [36]. To handle the strange-quark degrees of freedom in the nucleon, we must extend the model to flavor SU(3). However, this flavor SU(3) extension of the model needs to introduce only one additional parameter, i.e., the mass difference between the strange and nonstrange quarks [52,53]. This means that we can still make nearly parameter-free predictions for PDFs. This should be contrasted with variant species of meson-cloud (convolution) models, which are also believed to incorporate the nonperturbative chiral dynamics of QCD. In fact, the meson-cloud models contain quite a few model parameters, such as several meson-quark coupling constants, coupling form factors, parameters of parton distributions in the mesons, and so forth [54,55]. Moreover, the model predictions often depend critically on how many meson-baryon intermediate states are included in the theoretical calculations. This last fact is sometimes a serious obstruction to giving unique and quantitatively trustable predictions on the sea-quark distributions in the nucleon. We emphasize again that the CQSM does not suffer from these bothersome problems, because it is nearly parameter free. As a matter of course, the biggest problem or shortcoming common to all the low-energy effective models of the nucleon including the CQSM is a lack of explicit gluon degrees of freedom. This point should always be kept in mind when applying low-energy models of the nucleon to the DIS physics, as we shall discuss later.

The main purpose of the present paper is to unravel the nonperturbative chiral dynamics of QCD hidden in the parton distribution functions of the nucleon through the analysis of the flavor structure of the nucleon seas. An important point is that the flavor structure of the nucleon seas including the strange-quark degrees of freedom is analyzed simultaneously for the unpolarized PDFs and for the longitudinally polarized PDFs within a single theoretical framework. This framework is the flavor SU(3) version of the CQSM, which contains only one adjustable parameter, i.e., the effective mass difference between the strange and nonstrange quarks. To get a feeling about the reliability of the model, we first carry out a systematic comparison between the model predictions and the results of the most recent unbiased global fits by the NNPDF Collaboration. In our opinion, this systematic comparison is of special importance. This is due to the fact that if one picks up only a specific distribution function, it would not be extremely difficult to reproduce the corresponding empirical distributions, especially using models like the meson-cloud models, which contain many parameters and degrees of freedom. Unfortunately, it sometimes happens that such an agreement is fortuitous and the same model with the same set of parameters fails to reproduce other independent distributions. This is the reason why we believe it is important to check how well a particular model can or cannot reproduce a wide class of empirical PDFs simultaneously.

We also investigate the charge-symmetry-violating (CSV) effects in the parton distribution functions based on exactly the same theoretical framework. The motivation to investigate the CSV effects in the nucleon parton distributions is as follows. In order to resolve the widely known anomaly of the Weinberg angle of the electroweak standard model raised in the analysis of the neutrino-induced DIS measurements by the NuTeV group [56,57], two mechanisms from QCD are believed to play important roles: the asymmetry of the strange- and antistrange-quark distributions in the nucleon, and the CSV effects in the valence-quark distributions in the proton and the neutron. Which of these ingredients is more important is not a completely settled issue [58–72]. We believe that an analysis of the s-$\bar{s}$ asymmetry and the CSV distributions within a single theoretical framework would provide us with valuable information on the relative importance of these two mechanisms.

This paper is organized as follows. First, in Sec. II we try to estimate the reliability of the model by comparing the predictions of the SU(3) CQSM for the unpolarized PDFs with the recent global fits by the NNPDF Collaboration [73]. Next, we concentrate on inspecting the characteristic feature of the model predictions for the flavor structure of the unpolarized light-flavor sea-quark distributions, which has not been reliably determined on an observational basis alone. The characteristic predictions of the SU(3) CQSM are compared with the predictions of other models of the sea-quark distributions in the nucleon as well as with other empirical information if available. In Sec. III, a similar analysis is carried out for the longitudinally polarized PDFs, the global analyses of which was recently reported by the NNDPD Collaboration [74]. Next, in Sec. IV we investigate the CSV effects in the light-flavor quark and antiquark distributions within the framework of the SU(3) CQSM. An emphasis is put on getting useful information on the relative importance of the CSV effects and the strange- and antistrange-quark asymmetry in the resolution of the NuTeV anomaly of the Weinberg angle. Finally, we summarize what we have learned about the flavor structure of the nucleon seas in Sec. V.

II. FLAVOR SU(3) CQSM AND UNPOLARIZED PDFs

The theoretical formulation of the flavor SU(3) CQSM for evaluating the PDFs in a baryon was already described in detail in our previous papers [52,53]. [The SU(3) CQSM itself was first proposed in Ref. [75].] We therefore give

here only a brief sketch of it by focusing on its basic theoretical structure. The model Lagrangian of the flavor SU(3) CQSM is a straightforward extension of the SU(2) one. It is given by

$$\mathcal{L} = \mathcal{L}_0 + \mathcal{L}_{\rm SB}, \tag{1}$$

where

$$\mathcal{L}_0 = \bar{\psi}(x)(i\partial\!\!\!/ - MU^{\gamma_5}(x))\psi(x), \tag{2}$$

with

$$U^{\gamma_5}(x) = e^{i\gamma_5\pi(x)/f_\pi}, \qquad \pi(x) = \pi_a(x)\lambda_a \quad (a = 1, \ldots, 8) \tag{3}$$

being the SU(3) symmetric part of the Lagrangian, while

$$\mathcal{L}_{\rm SB} = -\bar{\psi}(x)\Delta m_s P_s \psi(x), \tag{4}$$

with

$$\Delta m_s P_s = \begin{pmatrix} 0 & 0 & 0 \\ 0 & 0 & 0 \\ 0 & 0 & \Delta m_s \end{pmatrix} \tag{5}$$

is the SU(3) symmetry-breaking (SB) part resulting from the mass difference between the strange and nonstrange quarks. (Here, we neglect the light-quark masses so that $\Delta m_s \equiv m_s - m_{u,d} = m_s$.) The above effective Lagrangian contains eight meson fields [instead of three as in the case of the flavor SU(2) model]. However, we recall that in the framework of the CQSM these meson fields are not independent fields of quarks, as inferred from the fact that there is no kinetic term for the meson fields in the above basic Lagrangian of the model.

The fundamental dynamical assumptions of the model are as follows.

(i) First, the lowest-energy classical solution (or the mean-field solution) is obtained by embedding the SU(2) mean-field solution of hedgehog shape into the SU(3) matrix. [The same dynamical assumption is also used in the more familiar SU(3) Skyrme model [76–78].]

(ii) The second is the SU(3) symmetric quantization of the rotational motion in the collective coordinate space.

(iii) The third is the perturbative treatment of the SU(3) symmetry-breaking mass term. We recall that this mass difference Δm_s between the strange and nonstrange quarks is *the only parameter* of the model.

We fix this single parameter as follows. The mass difference is taken as an adjustable parameter in the physically reasonable range $m_s = 80$–120 MeV. As a general rule, the distribution functions for the light-flavor u and d quarks are generally rather insensitive to the value of Δm_s. As naturally expected, the strange-quark distributions are the most sensitive to the value of Δm_s. We found that an overall good reproduction of the shape of the empirical strange-quark distribution $s(x) + \bar{s}(x)$ is obtained with the choice $\Delta m_s = 80$ MeV. We therefore fix the value of Δm_s to be 80 MeV and continue to use this value in all of the following calculations. This means that there are no remaining free parameters in the model.

Before discussing the predictions of the SU(3) CQSM for the unpolarized PDFs in comparison with the empirical information given at high-energy scales, we think it is important to explain our general strategy for applying an effective model to DIS physics. It is widely believed that the predictions of effective models of hadrons should be taken as those given in the low-energy domain of nonperturbative QCD, while the parton distribution functions extracted from experiments correspond to the high-energy scale of perturbative QCD. A difficult question is how to harmonize these two domains of QCD. It is customarily assumed that the model predictions for PDFs given at the low-energy scale can be related to empirically extracted PDFs at high energy through the QCD evolution equation. The central difficulty we encounter here is a matching scale problem. That is, it is far from trivial how to specify the exact model energy scale from which one starts the evolution as above. Most effective models of baryons—like the MIT bag model or the meson cloud models—use a fairly low starting energy $Q^2_{\rm ini} \simeq 0.16$ GeV^2. On the other hand, there is some argument that the starting energy of the CQSM should be taken to be a little higher. In fact, we recall here the argument by Petrov *et al.* based on the instanton picture of the QCD vacuum [79,80], which is thought to give a theoretical foundation for the CQSM. According to them, the scale of the CQSM is set by the inverse of the average instanton size ρ as $Q_{\rm ini} \sim 1/\rho \sim 600$ MeV. Although reasonable, it seems to us that the relation between the choice of the initial scale and the average instanton size is very qualitative. It just indicates that any choice between $Q^2_{\rm ini} \simeq 0.3$ GeV^2 and $Q^2_{\rm ini} \simeq 0.4$ GeV^2 would be equally suitable. A fully satisfactory choice of the initial energy scale of evolution would be obtained only when one carries out a proper renormalization procedure of nonperturbative QCD, as is actually done in the framework of lattice QCD, although the calculation of the PDFs is not yet possible in this promising framework. (Another advantage of the lattice QCD treatment is that the renormalization is carried out at a fairly high-energy scale, i.e., $Q^2 = 4$ GeV^2, where one can safely start the perturbative evolution to higher energy scales.) Even though there is a theoretical indication that the model scale of the CQSM is higher than that of other effective models of baryons, it is still much smaller than the scale of 1 GeV, so that some sensitivity of the final predictions on the choice of the initial scale of evolution cannot be completely

avoided. For instance, we find that the two choices $Q^2_{\rm ini} = 0.30\ {\rm GeV}^2$ and $Q^2_{\rm ini} = 0.40\ {\rm GeV}^2$ cause a difference in the range of 4–8% for the heights of valence-like peaks of the unpolarized PDFs at $Q^2 = 2\ {\rm GeV}^2$. Since better agreement with the empirical PDFs is obtained with the choice $Q^2_{\rm ini} = 0.30\ {\rm GeV}^2$, we continue to use this value, which was the value used in our previous studies [50–53].

In any case, we emphasize again that the value $Q^2_{\rm ini} = 0.30\ {\rm GeV}^2$ that we use as the initial scale of evolution in the CQSM is a little higher than the value $Q^2_{\rm ini} \simeq 0.16\ {\rm GeV}^2$ frequently used in many effective models of baryons, like the MIT bag model or the meson cloud models. This difference is sometimes critical, because the validity of using the perturbative evolution equation at too low energy scales is a delicate question. In fact, we show in Fig. 1 the QCD running coupling constant at the next-to-leading order (NLO) as a function of Q^2. (Here we have used the exact solution of the NLO evolution equation with the standard minimal subtraction scheme in the fixed-flavor scheme with $n_f = 3$ even beyond the charm threshold. However, the effects of charm on the quantity discussed here would be very small as compared with the necessary precision of our discussion.) One sees that the α_S at the scale of $Q^2 = 0.16\ {\rm GeV}^2 = (400\ {\rm MeV})^2$ already shows a diverging behavior, which casts some doubt on the use of the perturbative renormalization group equation at such scales. On the other hand, at the initial energy scale of the CQSM, i.e., at $Q^2 = 0.30\ {\rm GeV}^2 \simeq (550\ {\rm MeV})^2$, perturbative QCD may be barely applicable. [Whether the value of $\alpha_S \simeq 0.84$ at the scale $Q^2 = 0.30\ {\rm GeV}^2$ is large or small is a delicate question. However, a more transparent measure of the applicability of the perturbative renormalization group equation is provided by the change rate of α_S as a function of Q^2, which can be easily determined. Another remark is that, if one uses the leading-order (LO) evolution equation, the diverging behavior of $\alpha_S(Q^2)$ appears at a lower energy scale. This is one of the reasons why many low-energy models, like the MIT bag model or the meson cloud models, adopt the LO evolution equation together with a very low starting energy of evolution. However, since the main purpose of our analysis is to compare the predictions of the SU(3) CQSM with the NNPDF fits carried out at NLO, the consistency requires us to use the evolution scheme at NLO.)

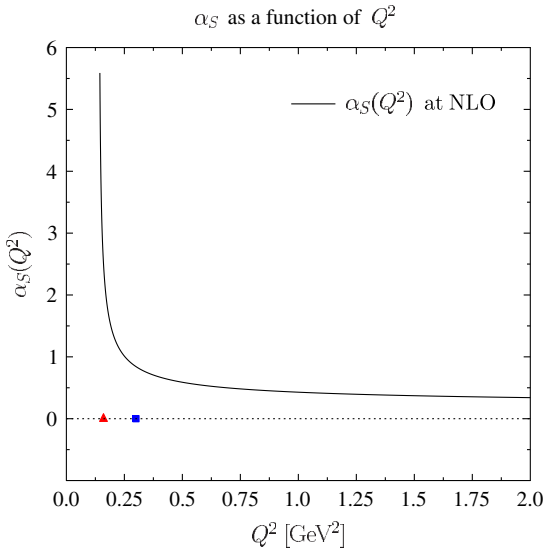

FIG. 1 (color online). The QCD running coupling constant $\alpha_S \equiv g^2/4\pi$ at NLO as a function of Q^2. The filled (red) triangle corresponds to the frequently used starting energy scale of evolution in the MIT bag model or meson cloud models, whereas the filled (blue) square corresponds to the starting energy scale used in the CQSM.

As shown above, although our choice of a slightly higher starting energy of evolution is preferable from the standpoint of using the perturbative renormalization group equation, there is one thing that we must pay attention to. The key quantities in our argument here are the momentum fractions of quarks and gluons as functions of the energy scale Q^2. Up to this time, the momentum fractions of quarks and gluons in the nucleon at the high-energy scale are fairly precisely known. Given below are the empirical values for the quark and gluon momentum fractions $\langle x\rangle^Q$ and $\langle x\rangle^G$ given at $Q^2 = 4\ {\rm GeV}^2$ by the MRST2004 analysis [81,82]:

$$\langle x\rangle^Q = 0.579, \qquad \langle x\rangle^G = 0.421. \tag{6}$$

Here, for simplicity, we have neglected very small error bars. As an interesting trial, we carried out a *downward evolution* of the quark and gluon momentum fraction by starting with these known empirical values at the high-energy scale. The results are shown, respectively, by the solid and the long-dashed curves in Fig. 2.

As anticipated, as Q^2 decreases the quark momentum fraction $\langle x\rangle^Q$ increases, whereas the gluon momentum fraction $\langle x\rangle^G$ decreases, eventually becoming zero at a certain energy scale [83,84]. An important observation here is the fact that, at the model energy scale of the CQSM, i.e., $Q^2 = 0.30\ {\rm GeV}^2 \simeq (550\ {\rm MeV})^2$, the gluon still carries about 20% of the nucleon momentum. Since the CQSM is an effective quark model—which does not contain explicit gluon degrees of freedom—to start the evolution at $Q^2 = 0.30\ {\rm GeV}^2$ amounts to neglecting the important role of gluons, which are likely to carry about 20% of the nucleon momentum even at this relatively low-energy scale. We will show later that this observation has an important phenomenological consequence in the interpretation of the predictions of the CQSM evolved to the high-energy scales.

Before proceeding further, it would be fair to refer to another limitation of the CQSM. The limitation is due to a general restriction from the limit of a large number of colors

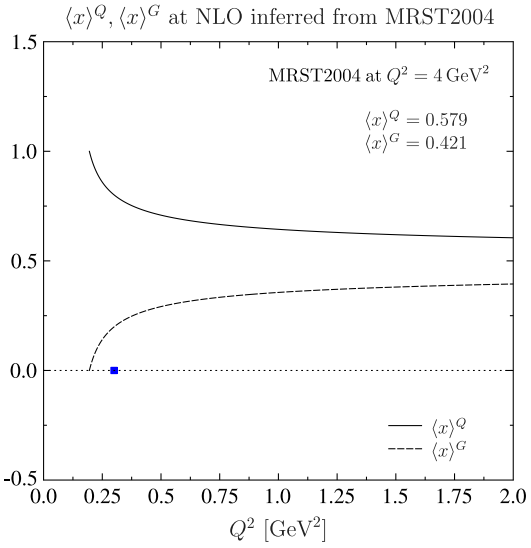

FIG. 2 (color online). The quark and gluon longitudinal momentum fractions as functions of Q^2, obtained by solving the QCD evolution equation at NLO with the initial conditions $\langle x\rangle^Q = 0.579$ and $\langle x\rangle^G = 0.421$ given at $Q^2 = 4$ GeV^2 by the MRST2004 analysis [81,82]. The filled (blue) square corresponds to the starting energy scale used in the CQSM.

N_c. As argued by Diakonov *et al.* [43,80], the CQSM provides a practical realization of large-N_c QCD, so that the parton distribution functions depend on the Bjorken variable x in such a way that $N_c x = O(1)$ in the limit $N_c \to \infty$. Since $N_c = 3$ in nature, this dictates that the CQSM is a good approximation to QCD only in the region of "not too small" x in order to comply with the above scaling law. A more concrete argument on the applicability range of x was provided by Petrov *et al.* [85]. Since the CQSM is an effective theory of QCD, which is not renormalizable, it needs a physical cutoff. An effective regularization energy Λ_{cut} is provided by the inverse of the average instanton size ρ as $\Lambda_{\mathrm{cut}} \sim 1/\rho \sim 600$ MeV. Petrov *et al.* argued that, in the region $x \leq (M/\Lambda_{\mathrm{cut}})/N_c \simeq 0.1$, the model predictions for the parton distributions are sensitive to the cutoff energy and/or the detail of the regularization method, and as such they are not necessarily reliable. In the following study, we take the less ambitious and more pragmatic standpoint that the CQSM is one of the effective models of baryons (like the MIT bag model or the meson cloud models), and we will show the predicted PDFs in the whole range of x, i.e., $0 < x < 1$, although the above caution should be kept in mind.

Now we are in a position to compare the predictions of the SU(3) CQSM for the unpolarized PDFs with the empirically extracted ones. First, to get a feeling about the degree of success or failure of the model, we compare our predictions with the recent unbiased global fits of unpolarized PDFs by the NNPDF Collaboration. (Here, we use the NNPDF NLO2.1 fits at NLO with $n_f = 3$ [73].) The NNPDF fits are given at $Q^2 = 2$ GeV^2 for the following combinations of the PDFs:

(i) the singlet distribution, $\Sigma(x) \equiv \sum_{i=1}^{n_f}(q_i(x) + \bar{q}_i(x))$;
(ii) the gluon, $g(x)$;
(iii) the total valence, $V(x) \equiv \sum_{i=1}^{n_f}(q_i(x) - \bar{q}_i(x))$;
(iv) the nonsinglet triplet, $T_3(x) \equiv (u(x) + \bar{u}(x)) - (d(x) + \bar{d}(x))$;
(v) the sea asymmetry distribution, $\Delta_S(x) \equiv \bar{d}(x) - \bar{u}(x)$;
(vi) the strange-antistrange sum, $S^+(x) \equiv s(x) + \bar{s}(x)$;
(vii) the strange-antistrange difference, $S^-(x) \equiv s(x) - \bar{s}(x)$.

In order to make a comparison, the CQSM predictions given at the initial scale $Q^2_{\mathrm{ini}} = 0.30$ GeV^2 are evolved to the corresponding scale of $Q^2 = 2$ GeV^2 by using the evolution equations at NLO.

Figure 3 shows the comparison for the PDFs $xT_3(x)$, $x\Delta_S(x)$, $xS^+(x)$, and $xS^-(x)$. We find fairly good agreement between the theory and the NNPDF fits for the flavor-nonsinglet triplet distribution $T_3(x)$ and the light-flavor sea asymmetry $\Delta_S(x)$. The detailed inspection reveals that the agreements are not perfect. However, in view of the almost parameter-free nature of the model, this agreement can be taken as one of the nontrivial successes of the CQSM, which properly takes account of the chiral dynamics of QCD. [Incidentally, we stress that the distributions $T_3(x)$ and $\Delta_S(x)$ are quite insensitive to the value of Δm_s.]

Turning to the strange distributions, we find that the model prediction for $S^+(x) = s(x) + \bar{s}(x)$ appears to overestimate the NNPDF fit by roughly a factor of 2. This feature of the model prediction is anticipated. As was intensively discussed for the SU(3) Skyrme model, the SU(3)-symmetric collective quantization supplemented with the perturbative treatment of the SU(3)-breaking mass-difference term [which is used in our treatment of the SU(3) CQSM] is in danger of overestimating the effects of kaon clouds, which might in turn lead to an overestimation of the strange-quark components in the nucleon [86–88]. We conjecture that plausible predictions for the strange and antistrange distributions in the nucleon would lie just between the predictions of the SU(3) CQSM and the SU(2) CQSM, which amounts to multiplying the SU(3) CQSM predictions for $s(x)$ and $\bar{s}(x)$ by a factor of $1/2$. As a matter of fact, the reduction factor of just $1/2$ has no strict foundation and is *ad hoc*. It can be any number between 1 and 0. In principle, this reduction factor can be treated as an additional parameter of the model. However, there is no absolutely trustworthy empirical information to fix this parameter. We therefore simply say that—as seen from Fig. 3—after multiplying by this reduction factor of $1/2$, the model prediction for $S^+(x)$ is consistent at the order-of-magnitude level with the current NNPDF fit, except for the larger-x region where the NNPDF fit does not necessarily respect the positivity of the distribution.

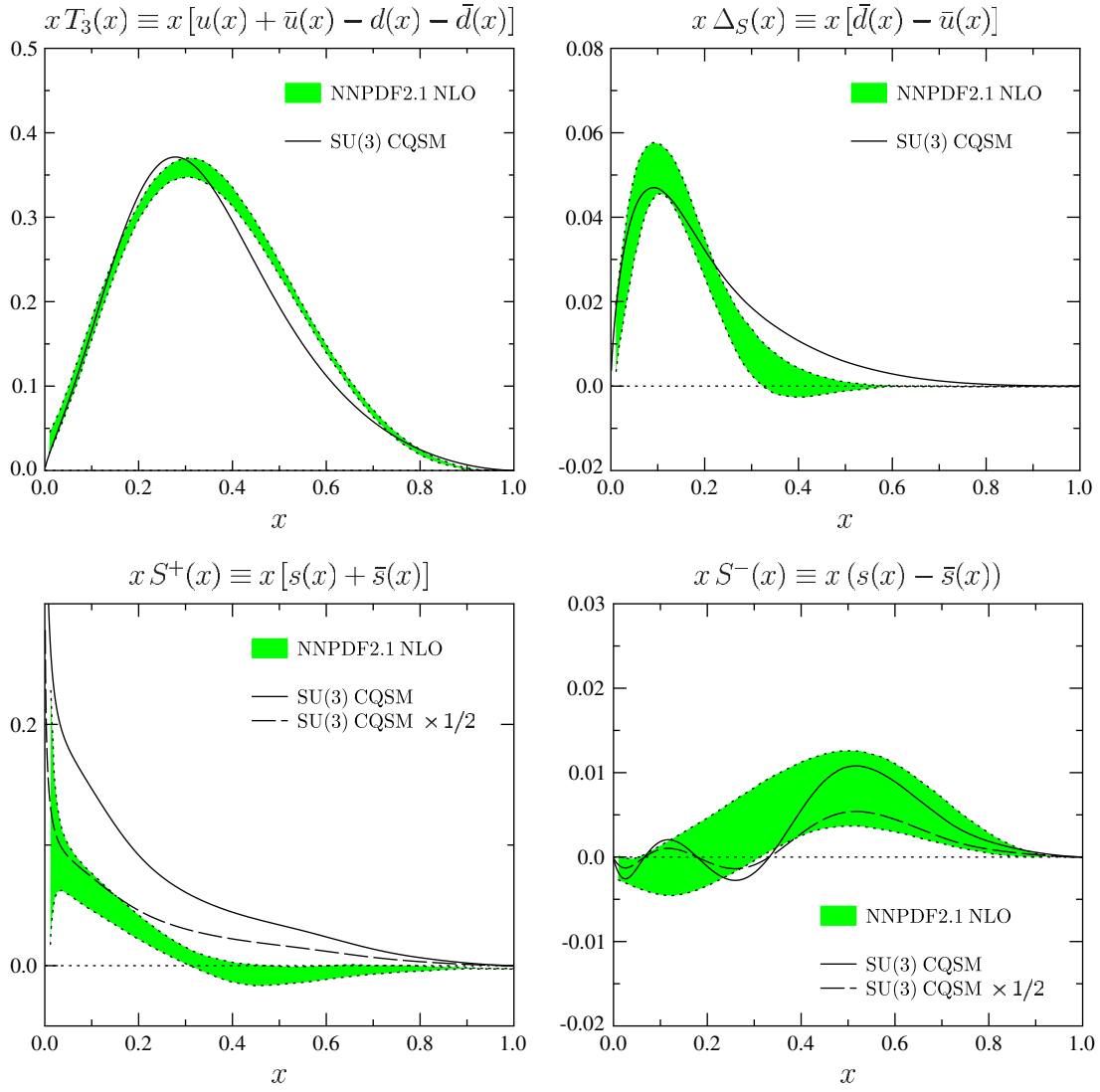

FIG. 3 (color online). The predictions of the SU(3) CQSM for the nonsinglet and strange-quark distributions evolved from $Q^2_{\rm ini} = 0.30$ GeV^2 to $Q^2 = 2$ GeV^2 in comparison with the NNPDF2.1 NLO global fits shown by the shaded areas [74]. The solid curves are the predictions of the SU(3) CQSM. The long-dashed curves for the strange-quark distribution are the predictions of the SU(3) CQSM reduced by a factor of $1/2$ (see text).

Also very interesting is the asymmetry of the strange and antistrange distributions. A noteworthy feature of the NNPDF fit is that the difference distribution $xS^-(x) \equiv x[s(x) - \bar{s}(x)]$ has a peak around $x \sim 0.5$. Very curiously, this feature is perfectly consistent with the prediction of the SU(3) CQSM. The good agreement is not limited to the position of the peak. The absolute magnitude of the asymmetry is also consistent with the NNPDF fit. Note that the bare prediction of the SU(3) CQSM and the prediction reduced by a factor of $1/2$ are both consistent with the NNPDF fit within the uncertainty band, although we prefer the reduced prediction.

Next, in Fig. 4 we show the model predictions for the singlet distribution $\Sigma(x)$, the gluon distribution $g(x)$, and the net valence distribution $V(x)$ in comparison with the NNPDF fits. As compared with the success for the nonsinglet distributions, we find that the model prediction overestimates the NNPDF fit by about 20%. The reason for this discrepancy may be interpreted as follows. We already pointed out that, at the starting energy scale of evolution, the gluon field is likely to carry about 20% of the total nucleon momentum, which means that the quark fields carry only about 80% of the nucleon momentum. On the other hand, the CQSM is an effective quark model, which does not contain explicit gluon degrees of freedom; the net nucleon momentum is naturally saturated by the momenta of quarks and antiquarks at the model scale. Thus, we simply set the gluon distribution to zero at the starting energy scale of evolution, i.e., at $Q^2_{\rm ini} = 0.30$ GeV^2. This naturally fails to take into account the fact that the net

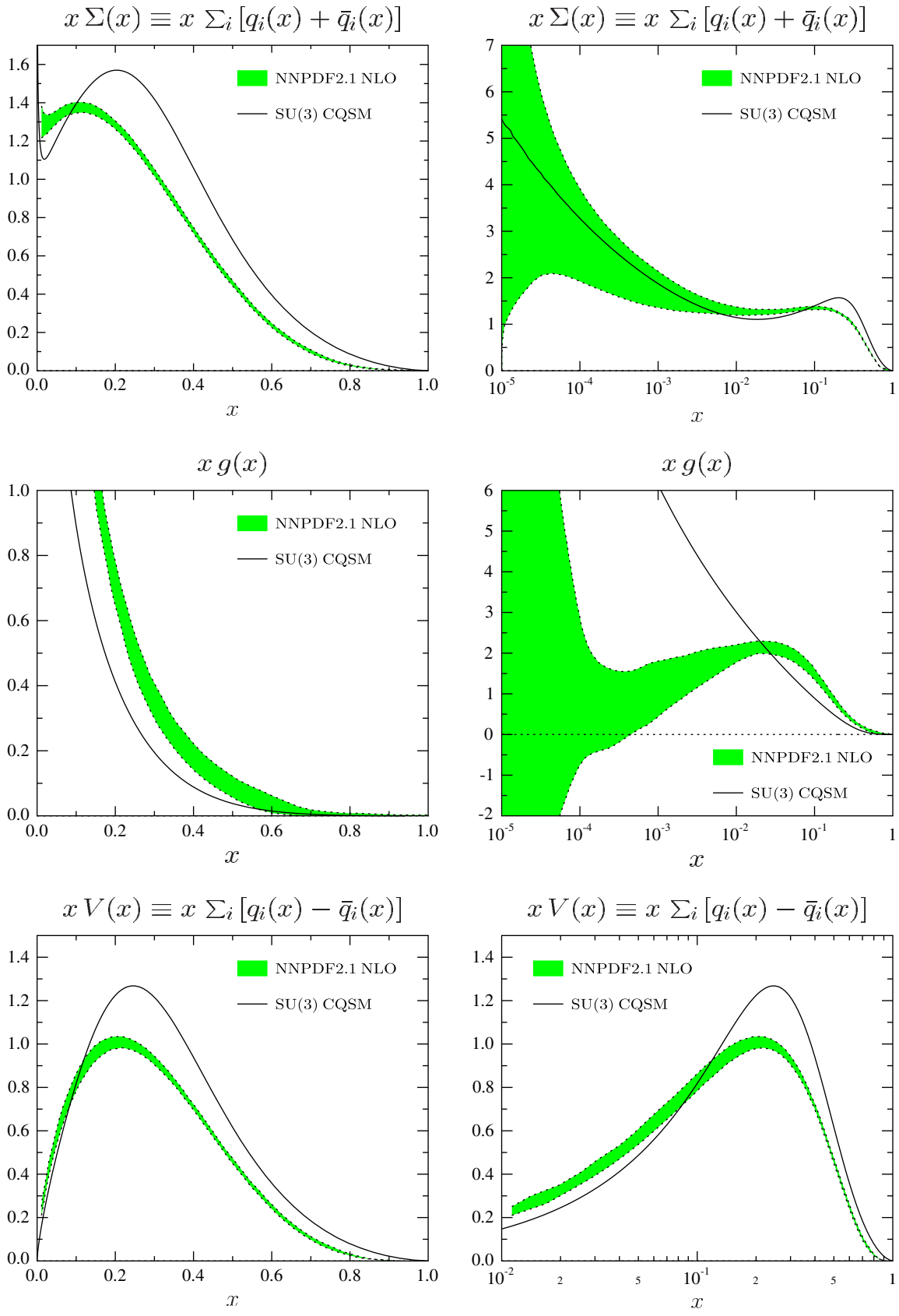

FIG. 4 (color online). The SU(3) CQSM predictions for the singlet quark, gluon, and valence-quark distributions in comparison with the NNPDF2.1 NLO fits.

momentum fraction of quarks at the initial scale must be only about 80%, which would then lead to an overestimation of the flavor singlet combination of the quark and antiquark distribution $\Sigma(x)$ by about 20%. For the same reason, we cannot expect that the model can give a reasonable description of the gluon distribution even though a nonzero gluon distribution is generated through evolution. Naturally, the gluon distribution obtained in this way has no valence-like peak like that observed in the empirical fit.

Turning to the total valence distribution $V(x)$, one again observes that the model prediction overestimates the NNPDF fit by about 20%. The reason for this overestimation is slightly more complicated than that for the singlet distribution $\Sigma(x)$. Since this distribution $V(x)$ is given as a difference of the quark and antiquark distributions, it does not couple to the gluon distribution at the process of evolution, which is different from the distribution $\Sigma(x)$. Still, since it is a symmetric sum of the three flavors (u, d, and s), the possible overestimation of the net distribution at the initial energy scale pointed out before is likely to remain at higher energy scales. Another possible reason would be that the model might still underestimate the sum of the light-flavor sea-quark distributions, i.e., $\bar{u}(x) + \bar{d}(x)$, which leads to an overestimation of the combination $u(x) - \bar{u}(x) + d(x) - \bar{d}(x) + s(x) - \bar{s}(x)$, provided that the contribution of $s(x) - \bar{s}(x)$ in this combination is small.

A lesson learned from the above analysis can be described as follows. The overall agreement between the SU(3) CQSM and the NNPDF2.1 NLO fits are fairly good in light of the nearly parameter-free nature of the model predictions. However, the agreement is not naturally perfect. The main reason for a discrepancy would be the neglect of the gluon degrees of freedom, which appear to play non-negligible roles in the flavor-singlet channel even at relatively low-energy scales. On the other hand, we shall see in the next section that the role of gluons at the low-energy model scale of the CQSM is likely to be much less important in the case of longitudinally polarized distributions.

Now that we have a feeling about the reliability of the model as well as its limitations (through the comparison with the unbiased global fits of the unpolarized PDFs by the NNPDF groups), we turn our attention to a more detailed inspection of the flavor structure of the sea-quark (-antiquark) distributions in the nucleon. To unravel the underlying physics, a comparison with related theoretical investigations (as well as other experimental information if available) is particularly instructive. First, we call attention to the strange distribution $s(x) + \bar{s}(x)$ in the nucleon extracted from the analysis of charged kaon production in SIDIS by the HERMES Collaboration [25]. As is widely known, the extracted $s(x) + \bar{s}(x)$ distribution appears to have an intriguing two-component structure as illustrated in Fig. 5. Here, following Ref. [89], the HERMES data with $x < 0.1$ are represented by the open circles, while those with $x > 0.1$ are represented by the filled black circles.

The observed two-peaked structure motivated Chang and Peng to introduce an interesting physical interpretation, to be explained below [89]. (See also the more recent paper by Chang, Cheng, Peng, and Liu [90].) Their interpretation is based on the idea of intrinsic charm in the nucleon, which was proposed many years ago by Brodsky, Hoyer, Petesen, and Sakai (BHPS model) [91,92]. According to BHPS, the intrinsic sea is a component that is expected to have a valence-like peak at larger x, while the extrinsic sea is thought to be generated through QCD splitting processes. Inspired by this idea, Chang and Peng proposed an idea that $x > 1$ HERMES data are dominated by an "intrinsic" sea, while $x < 0.1$ data are from an "extrinsic" sea [89]. According to them, a component of the HERMES data, which has a peak around $x \sim 0.1$–0.3 can be reproduced by the intrinsic five-quark model (see the solid curve in Fig. 5) with the mixing rate $P_5^{uuds\bar{s}} \simeq 0.024$ for the five-quark component in the nucleon. At first sight, this appears to provide a reasonable explanation of the peak structure of $x[s(x) + \bar{s}(x)]$ in the higher-x region. However, the following question immediately arises. Admitting that accounting for the five-quark component nicely explains the peak structure at higher x, how can one explain the sea-like component in the lower-x domain? What is important to recognize here is the fact that the solid curve in Fig. 5 shows the theoretical prediction, which was obtained after taking account of the evolution effects by solving the evolution equation starting from the scale $Q^2_{\rm ini} = 0.25$ GeV. This means that, to explain the whole HERMES data including the lower-x behavior, one absolutely needs a significant sea-like component at the starting

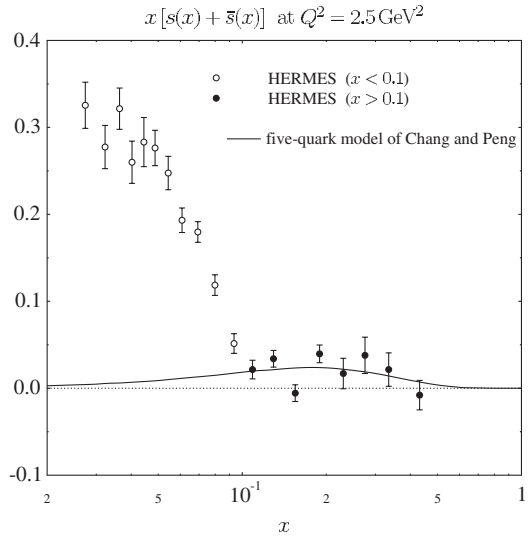

FIG. 5. HERMES's strange-quark distribution [25] in comparison with the prediction of the five-quark model of Chang and Peng [89], evolved to $Q^2 = 2.5$ GeV^2 from the initial scale of the model $Q^2_{\rm ini} = 0.25$ GeV^2.

energy scale. What generates these sea-like components? Assuming the correctness of the HERMES extraction, they must be higher Fock components of the nucleon state, like the seven-quark component, five-quark plus gluon, and so on. It is not absolutely clear whether the valence-like peak structure of the strange-quark distribution—which is obtained by confining to the lowest five-quark Fock component only—will remain after taking account of all the these higher Fock components of the nucleon wave function.

To answer the question raised above, we find it useful to look into the prediction of the SU(3) CQSM for the strange and antistrange distribution functions at the low-energy model scale. They are shown in Fig. 6. Very interestingly, the model predicts a sizable difference between the strange- and antistrange-quark distributions. The strange-quark distribution $xs(x)$ shows a two-component structure, i.e., the valence-like peak in the higher-x region and the sea-like component in the lower-x region. On the other hand, the antistrange-quark distribution has only a sea-like peak in the lower-x region. In particular, one finds that the s-quark distribution has a larger x component than the $\bar{s}$-quark distribution. Very interestingly, this feature is expected from the kaon cloud model of the nucleon advocated by Signal and Thomas [58], Burkardt and Warr [59], and also by Brodsky and Ma [60] many years ago. According to the kaon cloud picture, the strange- and antistrange-quark distributions in the proton are generated through the virtual dissociation process $p \to \Lambda + K^+$. In these virtual intermediate states, the s quark is contained in a baryon, i.e., in Λ, while the $\bar{s}$ quark is contained in a meson, i.e., in K^+. This is used to explain why the s quark has a harder valence-like component than the $\bar{s}$ quark [59,60]. Although we believe that this meson cloud picture gets straight to the point in a qualitative sense, not too much can be expected regarding its quantitative predictability because the meson cloud models generally contain too many adjustable parameters and large ambiguities. A great advantage of the CQSM is that it does not assume any explicit meson-baryon intermediate states, like the nucleon and pion, the nucleon and rho meson, the lambda and kaon, etc. Note that the above difference between the strange- and antistrange-quark distributions is an automatic consequence of the almost parameter-free calculation. Here, it is very important to recognize the fact that not only the valence-like component but also the sea-like component are generated as a consequence of solving the bound-state equation of the nucleon. In this sense, one can refer to the latter as an "intrinsic" sea but not an "extrinsic" sea, even though it is not a component with valence-like character. The point is that the basic theoretical framework of the CQSM is the mean-field theory (followed by the collective quantization of the zero-energy rotational modes), which enables us to incorporate infinitely many higher multiquark components in the language of perturbative Fock-space expansion. This argument indicates that the decomposition of the quark seas into "intrinsic" and "extrinsic" components is a strongly model-dependent or theoretical-scheme-dependent idea.

Also interesting here is the effect of evolution. We show in Fig. 7 the prediction of the SU(3) CQSM evolved to $Q^2 = 2.5\ \mathrm{GeV}^2$ corresponding to the HERMES SIDIS extraction of the distribution $x[s(x) + \bar{s}(x)]$. One sees that the trace of the valence-like peaked structure of the distribution $xs(x)$ still remains, albeit faintly. However, it is smoothly connected to the sea-like structure in the lower-x domain. Accordingly, we no longer see a clear

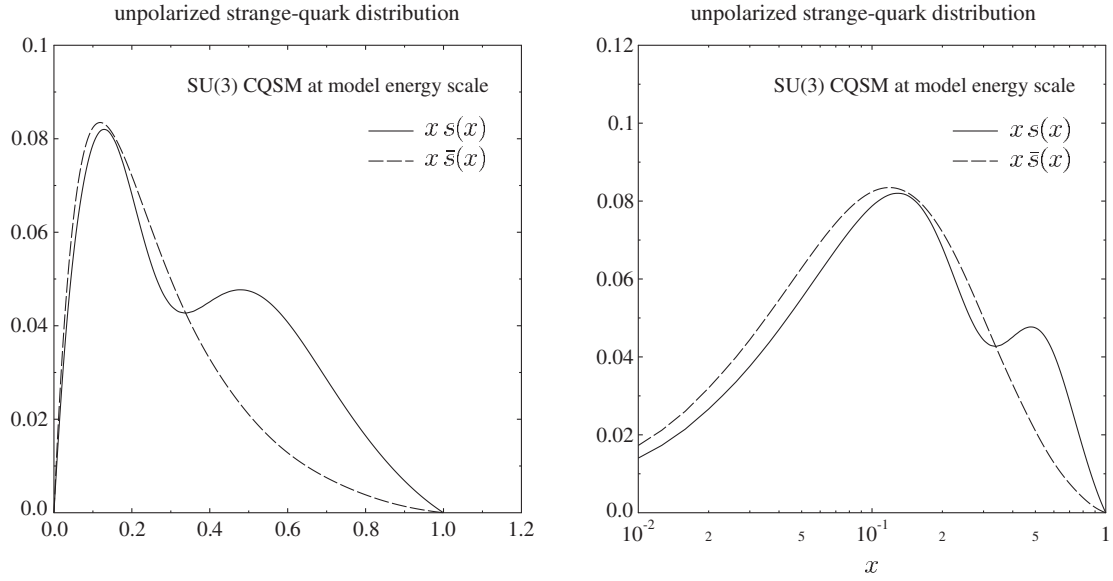

FIG. 6. The SU(3) CQSM predictions for the strange and antistrange distributions in the nucleon at the model energy scale. The left panel is in linear scale in x, while the right panel is in log scale.

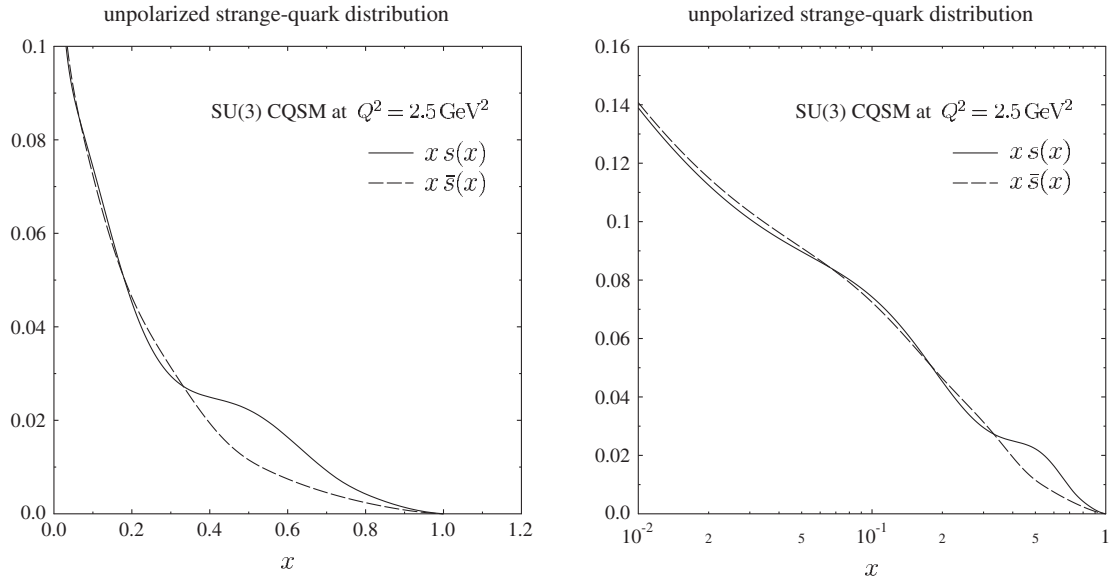

FIG. 7. The SU(3) CQSM predictions for the strange and antistrange distributions in the nucleon evolved to $Q^2 = 2.5$ GeV^2. The left panel is in linear scale in x, while the right panel is in log scale.

two-component structure in $xs(x)$. On the other hand, since the distribution $x\bar{s}(x)$ has only a sea-like component even at the low-energy model scale, the evolved distribution is simply sea-like.

After these considerations, it is instructive to compare the prediction of the strange- plus antistrange-quark distribution with the corresponding HERMES extraction as well as several other global fits. The filled black circles in Fig. 8 represent the HERMES SIDIS extraction for $x[s(x) + \bar{s}(x)]$. The thicker shaded area represents the NNPDF global fit given at $Q^2 = 2.0$ GeV^2, while the thinner shaded area is the CTEQ6.5 fit corresponding to $Q^2 = 2.5$ GeV^2. (Here, the NNPDF fit corresponds to a slightly lower scale, but the effect of this difference is expected to be small compared to the sizably large difference with the CTEQ6.5 fit.) The newer CT10 fit (dash-dotted curve) is also shown for reference. The bare prediction of the SU(3) CQSM is represented by the solid curve, whereas the reduced prediction of the SU(3) CQSM is represented by the long-dashed curve. (For the reason already explained, we prefer the reduced prediction for the strange-quark distributions.) As pointed out above, the SU(3) CQSM prediction for $x[s(x) + \bar{s}(x)]$ at $Q^2 = 2.5$ GeV^2 does not show any clear two-component structure, which is indicated by the HERMES data. Note that this is also a common feature of all the global fits including those of the NNPDF Collaboration and the CTEQ Collaboration. As is well known, the HERMES extraction of the strange distribution heavily depends on the expectation that our understanding of the semi-inclusive charged-kaon production mechanism is robust enough. Actually, the small-x data in the HERMES extraction corresponds to a relatively low-energy kinematical region, say, $Q^2 \sim 1$ GeV^2, where one would generally expect fairly large higher-twist corrections to the DIS analysis. Still another problem pointed out by Leader, Sidorov, and Stamenov is that the HERMES analysis uses the factorized QCD treatment of the data in a kinematical region where it is not necessarily justified [93]. We also point out that the

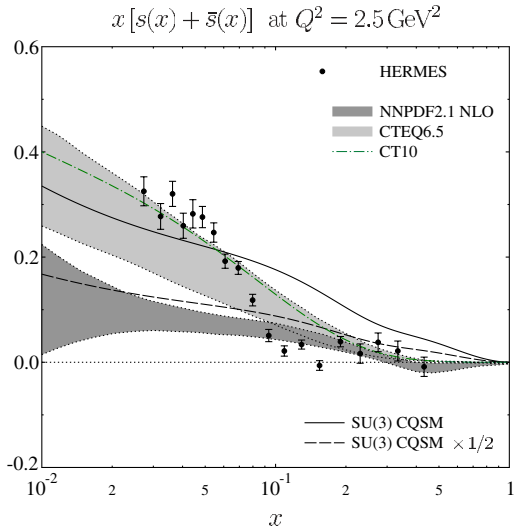

FIG. 8 (color online). The SU(3) CQSM predictions for the strange and antistrange distributions at $Q^2 = 2.5$ GeV^2 in comparison with the HERMES SIDIS extraction [25]. The solid curve is the bare prediction of the SU(3) CQSM, whereas the dashed curve is the prediction of the same model reduced by a factor of $1/2$. The global fits by the NNPDF Collaboration given at $Q^2 = 2$ GeV^2 and the two global fits by the CTEQ Collaboration corresponding to $Q^2 = 2.5$ GeV^2 are also shown for comparison [96,97].

most recent HERMES analysis [94], which is claimed to confirm their earlier analysis [25], was criticized in a recent paper by Stolarski [95]. Stolarski emphasized the importance of carrying out a careful analysis in which not only the multiplicity sum of the kaons but also that of the pion (as well as other combinations of K^+ and K^-) multiplicities are analyzed simultaneously. In any case, we strongly feel that some totally independent extraction of the strange-quark distributions—for example, by using the neutrino-induced inclusive DIS measurements—is highly desirable.

Chang and Peng pushed their idea of an "intrinsic" sea even further by considering the combination of the distributions $\bar{u}(x)+\bar{d}(x)-s(x)-\bar{s}(x)$ [98]. According to them, this combination is particularly interesting because the contribution from the "extrinsic" seas is expected to just cancel in this combination, so that it is only sensitive to the "intrinsic" sea. Their analysis goes as follows. First, they proposed to extract this distribution in an empirical way, i.e., by using the HERMES SIDIS data for $x[s(x)+\bar{s}(x)]$ at $Q^2=2.5\ \mathrm{GeV}^2$ [25] and the CTEQ6.6 fit for the distribution $x[\bar{u}(x)+\bar{d}(x)]$ at the same scale [96],

$$x[\bar{u}(x)+\bar{d}(x)-s(x)-\bar{s}(x)] \Rightarrow x[\bar{u}(x)+\bar{d}(x)]_{\mathrm{CTEQ6.6}} - x[s(x)+\bar{s}(x)]_{\mathrm{HERMES}}. \tag{7}$$

The resultant distribution is shown as filled circles in the left panel of Fig. 9. A prominent feature of the so-obtained $x[\bar{u}(x)+\bar{d}(x)-s(x)-\bar{s}(x)]$ is an expected valence-like peaked structure. Next, they calculated the corresponding distribution on the basis of the BHPS model [91,92], which gives

$$\bar{u}(x)+\bar{d}(x)-s(x)-\bar{s}(x) = P^{u\bar{u}}(x_{\bar{u}})+P^{d\bar{d}}(x_{\bar{d}}) - 2P^{s\bar{s}}(x_{\bar{s}}), \tag{8}$$

where $P^{Q\bar{Q}}(X_{\bar{Q}})$ is the x distribution of $\bar{Q}$ in the Fock component $|uudQ\bar{Q}\rangle$ of the nucleon state vector. In this calculation, they assumed that the probability of the intrinsic sea is proportional to $1/m_Q^2$, with m_Q being the mass of quark (antiquark) Q. This BHPS prediction is then evolved to $Q^2=2.5\ \mathrm{GeV}^2$ by taking $Q^2_{\mathrm{ini}}=(0.5\ \mathrm{GeV})^2$ as the initial energy scale of evolution. The result is shown by the solid curve in the left panel of Fig. 9. Chang and Peng emphasized that the qualitative agreement between the data and the calculation provides strong support for the existence of the intrinsic u- and d-quark seas and also for the adequacy of the BHPS idea.

We point out that the valence-like peaked structure of the empirically extracted distribution $x[\bar{u}(x)+\bar{d}(x)-s(x)-\bar{s}(x)]$ may critically depend on the following two factors:

(i) the two-component structure of the HERMES SIDIS data for $x[s(x)+\bar{s}(x)]$, and

(ii) the relative magnitudes of the sea-like components of the $\bar{u}+\bar{d}$ distribution and the $s+\bar{s}$ distribution in the lower-x domain.

To confirm this, we first check what happens if we do not use the HERMES SIDIS data for the strange-quark distribution. In fact, from the viewpoint of internal consistency, it would be more legitimate to extract the distribution

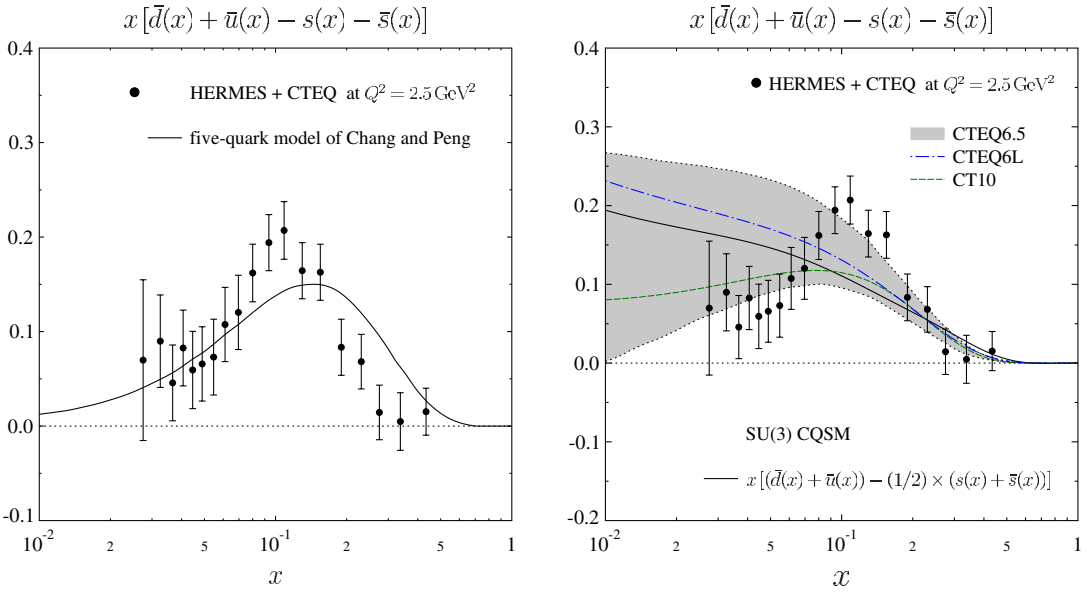

FIG. 9 (color online). The distribution $x[\bar{u}(x)+\bar{d}(x)-s(x)-\bar{s}(x)]$ obtained by using the CTEQ6.6 global fit for $\bar{u}+\bar{d}$ [96] and the HEREMES SIDIS data for $s+\bar{s}$ [25]. The left panel shows the comparison with the prediction of the BPHS five-quark model due to Chang and Peng [98], while the right panel shows the comparison with the prediction of the SU(3) CQSM as well as some other global fits [96,97].

in question by using the same extraction framework for both $x[\bar{u}(x)+\bar{d}(x)]$ and $x[s(x)+\bar{s}(x)]$. The dotted and dash-dotted curves in the right panel of Fig. 9 correspond to the results obtained by using the CTEQ6L fit [96] and the CT10 fit [97], respectively. One finds a big difference between these two fits. The distribution obtained from the CT10 fit has a peaked structure, whereas that obtained from the CTEQ6L does not. The origin of this difference can primarily be traced back to the relative magnitudes of the $s+\bar{s}$ and $\bar{u}+\bar{d}$ distributions in the lower-x region. (We point out that the CT10 fit gives a larger magnitude for the $s+\bar{s}$ distribution than either the CTEQ6L fit or the NNPDF fit.) For reference, we also show in the right panel of Fig. 9 the prediction of the CQSM (long-dashed curve). As explained before, we have used the reduced prediction for the $x[s(x)+\bar{s}(x)]$ distribution. It is interesting to see that the resultant distribution $x[\bar{u}(x)+\bar{d}(x)-s(x)-\bar{s}(x)]$ is remarkably similar in shape to that of the CTEQ6L fit, which does not show a peaked structure. In any case, all these theoretical and semiempirical predictions for the distribution $x[\bar{u}(x)+\bar{d}(x)-s(x)-\bar{s}(x)]$ lie within the wide uncertainty band indicated by the CTEQ6.5 fit, which in fact allows both peaked and peakless structures. Undoubtedly, to get more reliable information on the x dependence of this interesting combination $x[\bar{u}(x)+\bar{d}(x)-s(x)-\bar{s}(x)]$, we need to get more reliable information on the light-flavor sea-quark distribution $x[\bar{u}(x)+\bar{d}(x)]$ and the strange-quark distribution $x[s(x)+\bar{s}(x)]$ in the nucleon.

The interesting idea of a "two-component" quark sea was also advocated by Liu and others based on the path-integral formulation or within the framework of lattice QCD [90,99,100]. According to them, the light-flavor u- and d-quark seas consist of the connected sea and the disconnected sea, while the strange as well as the charm sea comes only from the disconnected sea. On the basis of this idea, they carried out a phenomenological extraction of the connected and disconnected pieces of the light-flavor sea, $\bar{u}(x)+\bar{d}(x)$. They first assumed that the disconnected-sea component of the $\bar{u}(x)+\bar{d}(x)$ distribution is proportional to the $s(x)+\bar{s}(x)$ distribution,

$$\bar{u}^{ds}(x)+\bar{d}^{ds}(x)=\frac{1}{R}[s(x)+\bar{s}(x)], \tag{9}$$

with the proportionality constant

$$R=\frac{\langle x\rangle_{s+\bar{s}}}{\langle x\rangle_{u+\bar{u}(DI)}}=\frac{\langle x\rangle_{s+\bar{s}}}{\langle x\rangle_{\bar{u}^{ds}+\bar{u}^{ds}}}=0.857(40), \tag{10}$$

which they estimated from lattice data. Then, they extracted the connected-sea component of the $\bar{u}(x)+\bar{d}(x)$ distribution by using the CT10 PDF fit for $\bar{u}(x)+\bar{d}(x)$ and the HERMES SIDIS data for the strange-quark distribution $s(x)+\bar{s}(x)$,

$$\begin{aligned}\bar{u}^{cs}(x)+\bar{d}^{cs}(x)&\equiv[\bar{u}(x)+\bar{d}(x)]-[\bar{u}^{ds}(x)+\bar{d}^{ds}(x)]\\&=[\bar{u}(x)+\bar{d}(x)]_{\mathrm{CT10}}\\&\quad-\frac{1}{R}[s(x)+\bar{s}(x)]_{\mathrm{HERMES}}.\end{aligned} \tag{11}$$

The connected and disconnected seas for $\bar{u}+\bar{d}$ extracted from the above-explained phenomenological analysis are shown in Fig. 10 by the filled squares and filled circles, respectively. Note that, by construction, the sum of these two components, i.e., the connected sea and the disconnected sea, coincides with the CT10 global fit shown by the dash-dotted curve. They emphasized that the connected-sea component so extracted appears to have a valence-like peak around $x\simeq 0.1$–0.2. However, it seems to us that their separation into the two components is not independent of the structure of the HERMES data for the strange-quark distribution. Going back to the original physical idea of Liu *et al.* [99,100], it is certainly true that the distribution $\bar{u}(x)+\bar{d}(x)$ is generally given as a sum of the connecte- and disconnected-sea contributions. This is similar to the idea of Chang and Peng [89,98]. In their language, it roughly corresponds to saying that the distribution $\bar{u}(x)+\bar{d}(x)$ consists of the "intrinsic" sea and the "extrinsic" sea. However, it should be recognized that there is no rigorous correspondence between the two terminologies, i.e., the idea of "intrinsic" and "extrinsic" seas and that of connected and disconnected seas in the language of lattice QCD. In fact, according to Chang and Peng, the strange-quark distribution $x[s(x)+\bar{s}(x)]$ also contains the "intrinsic" component. But this "intrinsic" sea requires at least a

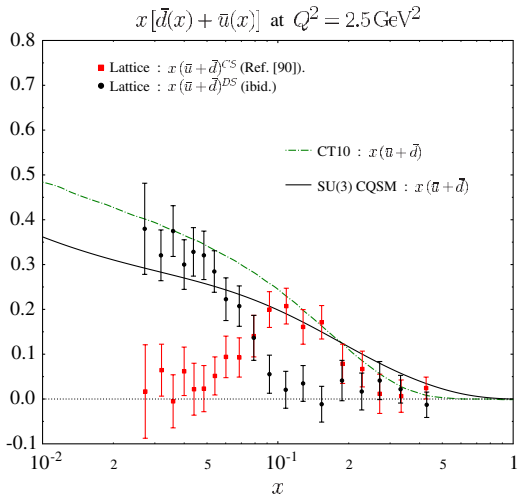

FIG. 10 (color online). The connected (filled circles) and disconnected (filled squares) seas for $\bar{u}(x)+\bar{d}(x)$ extracted from the CT10 PDF fit for $\bar{u}(x)+\bar{d}(x)$ [97] and the HERMES SIDIS data for the strange-quark distribution $s(x)+\bar{s}(x)$ [25], under the assumption that the disconnected-sea component of the $\bar{u}(x)+\bar{d}(x)$ distribution is proportional to the $s(x)+\bar{s}(x)$ distribution [90].

five-quark component, which needs to take account of disconnected seas within the framework of lattice QCD.

In our opinion, just like as the decomposition into the "intrinsic" and "extrinsic" seas is a model-dependent idea, the decomposition into the connected sea and the disconnected sea has a definite meaning only within the framework of lattice QCD. The only model-independent notion is the separation into quark and antiquark distributions. In fact, we show in Fig. 10 the prediction of the SU(3) CQSM for $x[\bar{u}(x)+\bar{d}(x)]$ (solid curve). Although it slightly underestimates the magnitude of $\bar{u}+\bar{d}$ in the small-x region as compared with the CT10 global fit [97], an important fact is that it does not show any two-component structure, similar to the CT10. Furthermore, within the framework of the CQSM, there is no idea of decomposing the antiquark distributions into two components (like the "intrinsic" and "extrinsic" seas). Both are contained within a single theoretical scheme without any separation between them. This reconfirms that the separation of the antiquark distribution into the "intrinsic" and "extrinsic" components or into the connected and disconnected seas is a *theoretical-scheme-dependent idea*, although we would never deny its usefulness for understanding the nature of quark seas in the nucleon.

III. FLAVOR SU(3) CQSM AND LONGITUDINALLY POLARIZED PDFs

In this section, we compare the predictions of the SU(3) CQSM for the longitudinally polarized PDFs with empirically extracted ones. Similarly as for the unpolarized PDFs, to get a feeling about the degree of success or failure of the model, we first compare our predictions with the recently reported global fits of the longitudinally polarized PDFs by the NNPDF Collaboration, i.e., NNPDFpol1.0 [74]. The NNPDF fits for the longitudinally polarized PDFs are given at $Q^2=1$ GeV^2 for the following combinations of the PDFs:

(i) the flavor singlet, $\Delta\Sigma(x)\equiv\sum_{i=1}^{n_f}(\Delta q_i(x)+\Delta\bar{q}_i(x))$;
(ii) the gluon, $\Delta g(x)$;
(iii) the isospin triplet, $\Delta T_3(x)\equiv(\Delta u(x)+\Delta\bar{u}(x))-(\Delta d(x)+\Delta\bar{d}(x))$;
(iv) the SU(3) octet, $\Delta T_8(x)\equiv\Delta u(x)+\Delta\bar{u}(x)+\Delta d(x)+\Delta\bar{d}(x)-2(\Delta s(x)+\Delta\bar{s}(x))$;
(v) the u plus $\bar{u}$, $\Delta u(x)+\Delta\bar{u}(x)$;
(vi) the d plus $\bar{d}$, $\Delta d(x)+\Delta\bar{d}(x)$;
(vii) the s plus $\bar{s}$, $\Delta s(x)+\Delta\bar{s}(x)$.

To make a comparison, the CQSM predictions are evolved from the initial scale $Q^2_{\rm ini}=0.30$ GeV^2 to the scale $Q^2=1.0$ GeV^2 where the NNPDF fits are given. As before, the gluon distribution at the initial scale is simply set to zero.

Figure 11 shows the comparison for the polarized PDFs $x\Delta T_3(x)$, $x\Delta T_8(x)$, $x\Delta\Sigma(x)$, and $x\Delta g(x)$. One can say that the agreement between the theoretical predictions and the global fits is fairly good—obviously much better than for the case of the unpolarized PDFs. From the similar analysis for the unpolarized distributions, we could have expected a good agreement for the nonsinglet distributions, like $\Delta T_3(x)$ and $\Delta T_8(x)$. However, as opposed from the unpolarized case, we clearly also get much better agreement for the flavor-singlet quark distribution $\Delta\Sigma(x)$ and the gluon distribution $\Delta g(x)$. Remember that, in the case of unpolarized PDFs, the flavor-singlet quark distribution was not reproduced very well. We argued that a possible reason for this discrepancy may be traced back to the neglect of the fact that the quark fields likely carry only about 80% of the nucleon momentum at the model scale of $Q^2_{\rm ini}\simeq 0.30$ GeV^2. Put another way, a good agreement for the flavor-singlet polarized distribution $\Delta\Sigma(x)$ indicates that the neglect of the gluon contribution at the model energy scale does little harm. Accordingly, the following picture emerges. At the low-energy scale corresponding to the CQSM, the gluon is likely to carry about 20% of the nucleon momentum fraction, but it carries negligibly small polarization. It is interesting to point out that this observation is consistent with the claim in the paper by Efremov, Goeke, and Pobylitsa [101]. In fact, on the general grounds of large-N_c QCD, they argued that the polarized gluon distribution is $1/N_c$ suppressed compared to the unpolarized one.

Note however that this does not mean that the gluon polarization remains small at high-energy scales. If the quark has a positive polarization at the low-energy scale, the polarization of gluons grows rapidly through the process of scale evolution. To get a feeling for the evolution effect, we solve the coupled evolution equation at NLO for the net quark polarization and the gluon polarization at NLO by starting with the initial condition of the CQSM, i.e., $\Delta\Sigma=0.35$ and $\Delta G=0.0$ at $Q^2_{\rm ini}=0.30$ GeV^2. The net gluon polarization ΔG obtained in this way is shown in Table I for some typical values of Q^2.

We see that, even if we assume that $\Delta G=0$ at the low-energy model scale, the gluon polarization increases rapidly as Q^2 becomes large. Very recently, the DSSV Collaboration carried out a systematic analysis of the gluon polarization in the nucleon by paying particular attention to the data offered by polarized proton-proton collisions available at the Relativistic Heavy Ion Collider [102]. The final answer from their new global fit, corresponding to the scale $Q^2=10$ GeV^2, is shown in Fig. 5 of their paper. This figure gives estimates for the 90% C.L. area in the plane spanned by the truncated moments of $\Delta g(x)$ calculated in $0.05\le x\le 1$ and $0.001\le x\le 0.05$. Their result can be summarized as

$$\int_{0.05}^{1}\Delta g(x)dx=0.194^{+0.060}_{-0.060} \tag{12}$$

and

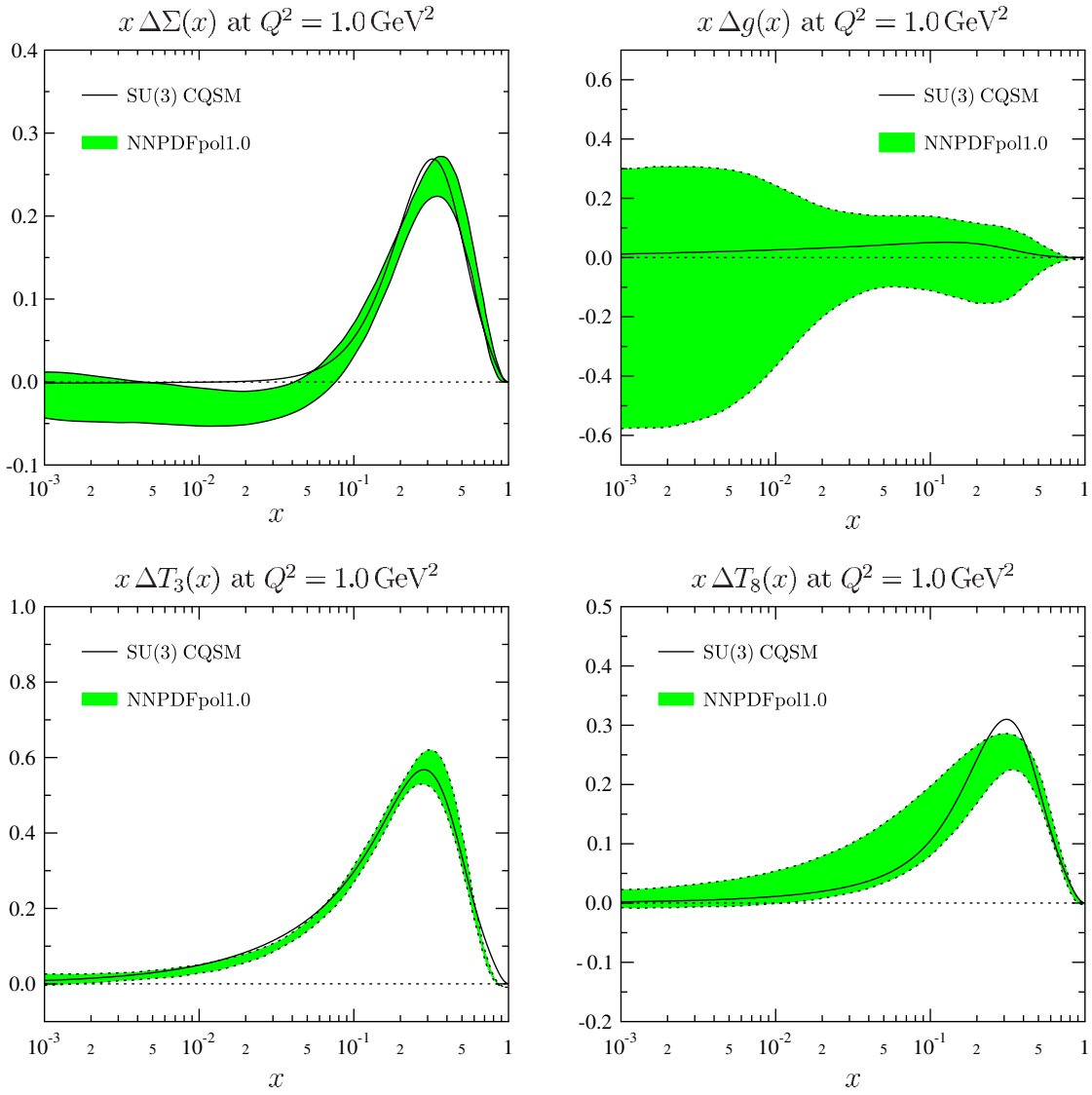

FIG. 11 (color online). The NNPDFpol1.0 fits for the polarized PDFs $x\Delta T_3(x)$, $x\Delta T_8(x)$, $x\Delta\Sigma(x)$, and $x\Delta g(x)$ in comparison with the predictions of the SU(3) CQSM.

$$\int_{0.001}^{0.05} \Delta g(x)dx = 0.166^{+0.062}_{-0.046.} \tag{13}$$

Summing up the contributions of both x regions, this would give

$$\int_{0.001}^{1} \Delta g(x)dx = 0.361^{+0.683}_{-0.522.} \tag{14}$$

TABLE I. The net longitudinal gluon polarization ΔG as a function of Q^2, obtained by solving the QCD evolution equation at NLO under the assumption that $\Delta G = 0$ and $\Delta\Sigma = 0.35$ at the initial energy scale of the CQSM.

$Q^2[\mathrm{GeV}^2]$	0.30	1.0	4.0	10.0
$\Delta G(Q^2)$	0.0	0.21	0.40	0.51

Note that the central value of the moment of $\Delta g(x)$, i.e., ΔG is positive with a sizable magnitude, although the negative value is not completely excluded due to the still large uncertainty coming from the integral in the small-x region. It is clear from the analysis above that a positive value of ΔG is theoretically more than natural. A difficult puzzle would arise if the results of global fits at the high-energy scale give a negative gluon polarization.

Next, in Fig. 12 we compare the prediction of the SU(3) CQSM for the distributions $x(\Delta u(x) + \Delta\bar{u}(x))$, $x(\Delta d(x) + \Delta\bar{d}(x))$, $x(\Delta s(x) + \Delta\bar{s}(x))$, and $x\Delta g(x)$ with the NNPDF fits, together with the slightly older DSSV08 global fits. One sees that the model predictions for $x(\Delta u(x) + \Delta\bar{u}(x))$ and $x(\Delta d(x) + \Delta\bar{d}(x))$ are remarkably consistent with both the NNPDF fits and the DSSV08 fits [103], which are close to each other anyway. What is problematic is the polarized strange-quark distribution.

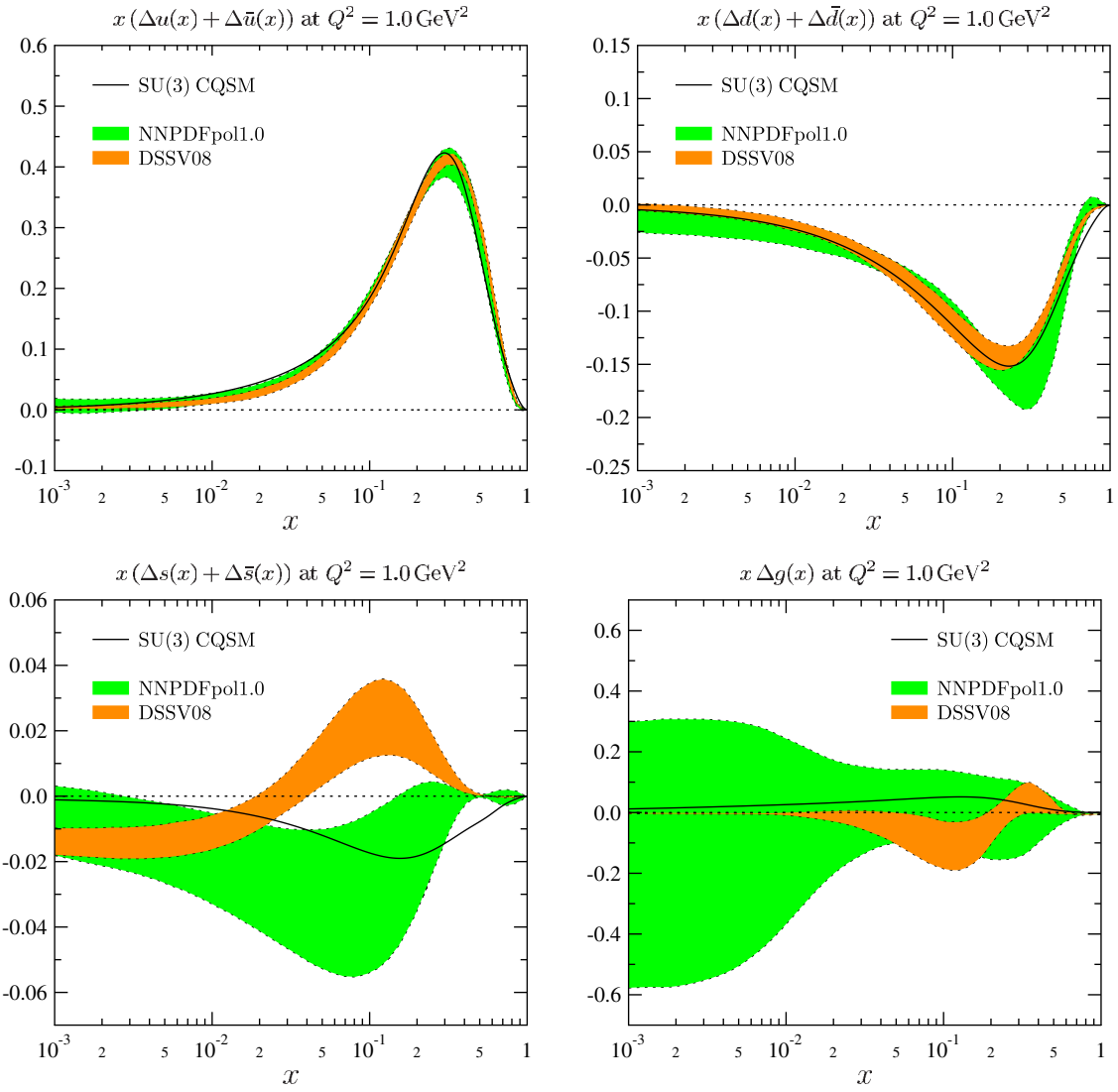

FIG. 12 (color online). The SU(3) CQSM predictions for the distributions $x(\Delta u(x)+\Delta\bar{u}(x))$, $x(\Delta d(x)+\Delta\bar{d}(x))$, $x(\Delta s(x)+\Delta\bar{s}(x))$, and $x\Delta g(x)$ in comparison with the NNPDFpol1.0 fits [74], together with the DSSV08 fits [103].

The NNPDF fit gives a negative strange-quark polarization, whereas the DSSV08 fit gives a positive polarization, at least in the larger-x region. This means that the presently available empirical information is not sufficient to determine the longitudinally polarized strange-quark distribution with confidence. The difference between the two determinations lies in the fact that the DSSV fits depend more heavily on the data of semi-inclusive DIS reactions. As we have already pointed out, we feel that our understanding of the mechanism of the semi-inclusive reactions has not reached a satisfactory level as compared with that of the inclusive DIS reactions. At any rate, it is interesting to point out that the prediction of the SU(3) CQSM for the strange-quark polarization is negative and consistent with the NNPDF fit, at least qualitatively. Finally, the shapes of the gluon distributions are also fairly different between the NNPDF fit and the DSSV08 fit. However, the uncertainty bands for $\Delta g(x)$ are sizably large in both fits. We point out that the prediction of the CQSM, obtained by assuming $\Delta g(x)=0$ at the model scale, is within the (broad) error band of the NNPDF fit.

After confirming that the predictions of the SU(3) CQSM for the longitudinally polarized PDFs are remarkably consistent with the empirically extracted PDFs—especially the NNPDFpol1.0 fit—we now turn to a more detailed inspection of the flavor structure of the longitudinally polarized sea-quark (-antiquark) distributions. We first show in Fig. 13 the predictions of the CQSM for the flavor (or isospin) asymmetry for the longitudinally polarized sea-quark distributions, i.e., $x(\Delta\bar{u}(x)-\Delta\bar{d}(x))$ in comparison with the DSSV09 fit. The thinner shaded area and the thicker shaded area are the allowed bands of the DSSV09 fit given at $Q^2=10\ \mathrm{GeV}^2$ with $\Delta\chi^2/\chi^2=2\%$ and $\Delta\chi^2=1$, respectively. The solid curve is the prediction

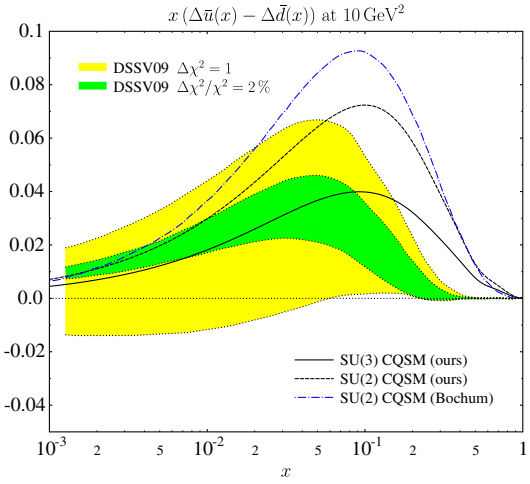

FIG. 13 (color online). The predictions of the SU(2) and SU(3) CQSM for the polarized light-flavor sea-quark asymmetry $x(\Delta\bar{u}(x) - \Delta\bar{d})$ in comparison with the DSSV09 global fit [105]. The dash-dotted curve is the prediction of the SU(2) CQSM by the Bochum group [104], whereas the long-dashed curve is our prediction in the same model. The prediction of the SU(3) CQSM is shown by the solid curve.

of the SU(3) CQSM, while the dashed curve is that of the SU(2) CQSM. The corresponding prediction of the Bochum group within the SU(2) CQSM is also shown for reference [104]. We first point out that our prediction and that of the Bochum group are sizably different in spite of the fact that they are based on the same SU(2) CQSM. The reason for this discrepancy is not absolutely clear. We conjecture that a possible reason is that their calculation used a schematic soliton profile function, while we use the solution of the self-consistent mean-field equation. Another reason may be that their predictions were obtained by using what they call the "interpolation formula," which is an approximate method of calculating PDFs or any nucleon observables within the framework of the CQSM [43]. In any case, our prediction for $\Delta\bar{u}(x) - \Delta\bar{d}(x)$ is significantly smaller than that of the Bochum group. Furthermore, the prediction of the SU(3) CQSM is much smaller than that of the SU(2) model. This provides a rare case in which the SU(3) CQSM and the SU(2) CQSM give significantly different predictions for the light-flavor u- and d-quark distributions. One can see that the prediction of the SU(3) CQSM is consistent at the order-of-magnitude level with the DSSV fit, although the positions of the peaks are slightly different. In any event, we find that the CQSM predicts a fairly large flavor (isospin) asymmetry not only for the unpolarized sea-quark distributions but also for the longitudinally polarized sea-quark distributions. This should be contrasted with the prediction of the meson cloud models. Although it is known that the meson cloud models nicely reproduce the isospin asymmetry of the unpolarized sea-quark distributions, their predictions for the longitudinally polarized sea-quark distributions are generally very small or even diverging.

The reason that $\Delta\bar{u}(x) - \Delta\bar{d}(x)$ is large was already discussed in several papers by Diakonov *et al.* [43,44]. According to their large-N_c argument, $u(x) - d(x)$ and also $\bar{u}(x) - \bar{d}(x)$ are $1/N_c$ suppressed as compared with $\Delta u(x) - \Delta d(x)$ and $\Delta\bar{u}(x) - \Delta\bar{d}(x)$, which was claimed to explain the fact that $\Delta\bar{u}(x) - \Delta\bar{d}(x)$ is large. However, in reality $N_c = 3$ and the explicit numerical calculation within the CQSM reveals that $\bar{u}(x) - \bar{d}(x)$ and $\Delta\bar{u}(x) - \Delta\bar{d}(x)$ actually have comparable magnitudes [52]. Furthermore, the large-N_c argument tells us little about the x dependencies of these distribution functions. The explicit x dependencies can be known only through explicit numerical calculation within the CQSM. To answer the above question beyond the simple large-N_c counting argument, we therefore think it is instructive to look more closely at the predictions of the CQSM for four basic twist-2 PDFs, i.e., the isoscalar and isovector combinations of the unpolarized and longitudinally polarized PDFs. [To avoid unnecessary complexity, we show here the predictions of the SU(2) CQSM. This is enough because the essential physics of strong spin-isospin correlation is already embedded in the SU(2) model in the form of a rotational symmetry-breaking mean field.]

In Fig. 14, the long-dashed curves stand for the contributions of the three valence quarks in the mean field, whereas the dash-dotted curves are those of the vacuum-polarized Dirac-sea quarks. The sums of these two contributions are shown by the solid curves. In this figure, the distribution functions in the negative-x region must be interpreted as antiquark distributions according to the rule

$$u(-x) + d(-x) = -[\bar{u}(x) + \bar{d}(x)], \tag{15}$$

$$u(-x) - d(-x) = -[\bar{u}(x) - \bar{d}(x)], \tag{16}$$

$$\Delta u(-x) + \Delta d(-x) = +[\Delta\bar{u}(x) + \Delta\bar{d}(x)], \tag{17}$$

$$\Delta u(-x) - \Delta d(-x) = +[\Delta\bar{u}(x) - \Delta\bar{d}(x)], \tag{18}$$

with $0 < x < 1$. The sign difference between the unpolarized and longitudinally polarized distributions originates from the symmetry properties under the charge-conjugation transformation. As one can see, the contributions of the three valence quarks have more or less similar shapes. They are peaked around $x \sim 0.2$–0.4. On the other hand, one sees totally different behaviors of the contributions of Dirac-sea quarks in different distribution functions, all of which are already known to play important roles in reproducing the empirical distributions. One may however notice that the Dirac-sea contributions are surprisingly similar in shape for the two isovector distributions, i.e., for $u(x) - d(x)$ and $\Delta u(x) - \Delta d(x)$. The fact that $u(x) - d(x) > 0$ in the negative-x region means that $\bar{u}(x) - \bar{d}(x) < 0$ for the

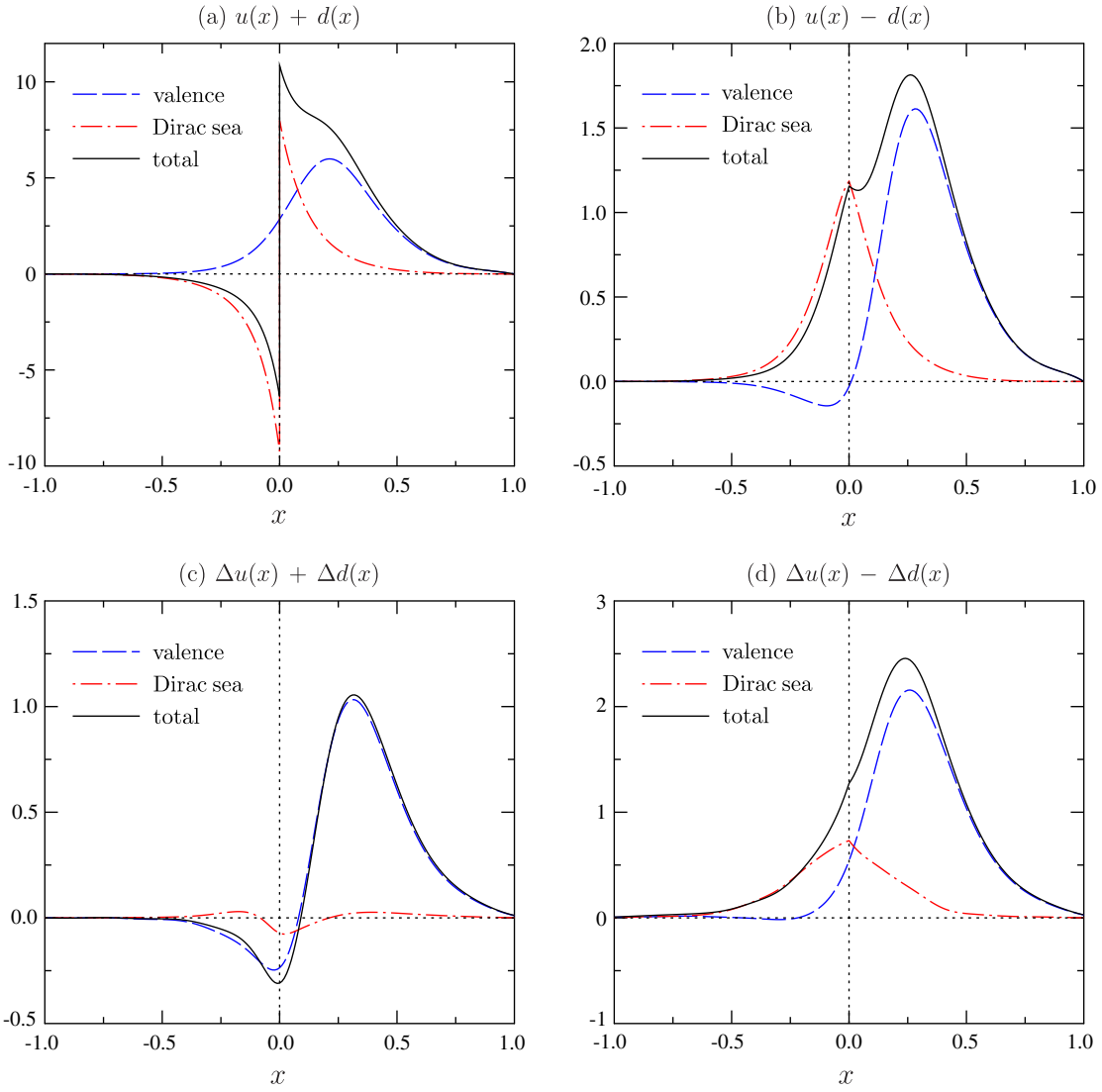

FIG. 14 (color online). The predictions of the SU(2) CQSM for the four basic twist-2 PDFs, i.e., the isoscalar and isovector combinations of the unpolarized and longitudinally polarized PDFs. The long-dashed curves are the contributions of the three valence quarks in the mean field, whereas the dash-dotted curves are those of the vacuum-polarized Dirac-sea quarks. The sums of these two contributions are shown by the solid curves.

physical value of x in the range $0 < x < 1$, which naturally explains the famous NMC observation. On the other hand, $\Delta u(x) - \Delta d(x) > 0$ in the negative-x region indicates that $\Delta\bar{u}(x) - \Delta\bar{d}(x) > 0$ for physical x. We recall that, in the energy spectrum of the single-particle Dirac equation for quarks under the hedgehog mean field, there are two (deformed) Dirac continuums: the positive-energy one and the negative-energy one. Here we concentrate on the negative-energy Dirac continuum and also on the Dirac-sea contribution to the PDFs in the negative-x region, which correspond to antiquark distributions. The strong similarity in the shapes of $u(x) - d(x)$ and $\Delta u(x) - \Delta d(x)$ in the negative-x region actually corresponds to anticorrelation, because of the rules (16) and (18). It appears that this anticorrelation is compatible with the grand spin-0 nature of the negative-energy Dirac continuum, although a more convincing argument is highly desirable. (We recall here the fact that the mean-field solution under the hedgehog potential is known to have a quantum number of $K = 0$, where $\boldsymbol{K} \equiv \boldsymbol{S} + \boldsymbol{T}$, with $\boldsymbol{S}$ and $\boldsymbol{T}$ being the ordinary spin and isospin operators, is called the grand spin operator.)

We have seen that the CQSM predicts a large flavor asymmetry not only for the unpolarized sea-quark distribution but also for the longitudinally polarized sea-quark distribution, i.e., $\Delta\bar{u}(x) - \Delta\bar{d}(x) > 0$. We are also interested in the polarized $\bar{u}$ and $\bar{d}$ seas. Shown in Fig. 15 are the predictions of the SU(3) CQSM in comparison with the DSSV09 fits [105]. For completeness, we also show a comparison for the polarized strange-quark distribution and the polarized gluon distribution, because they are also given

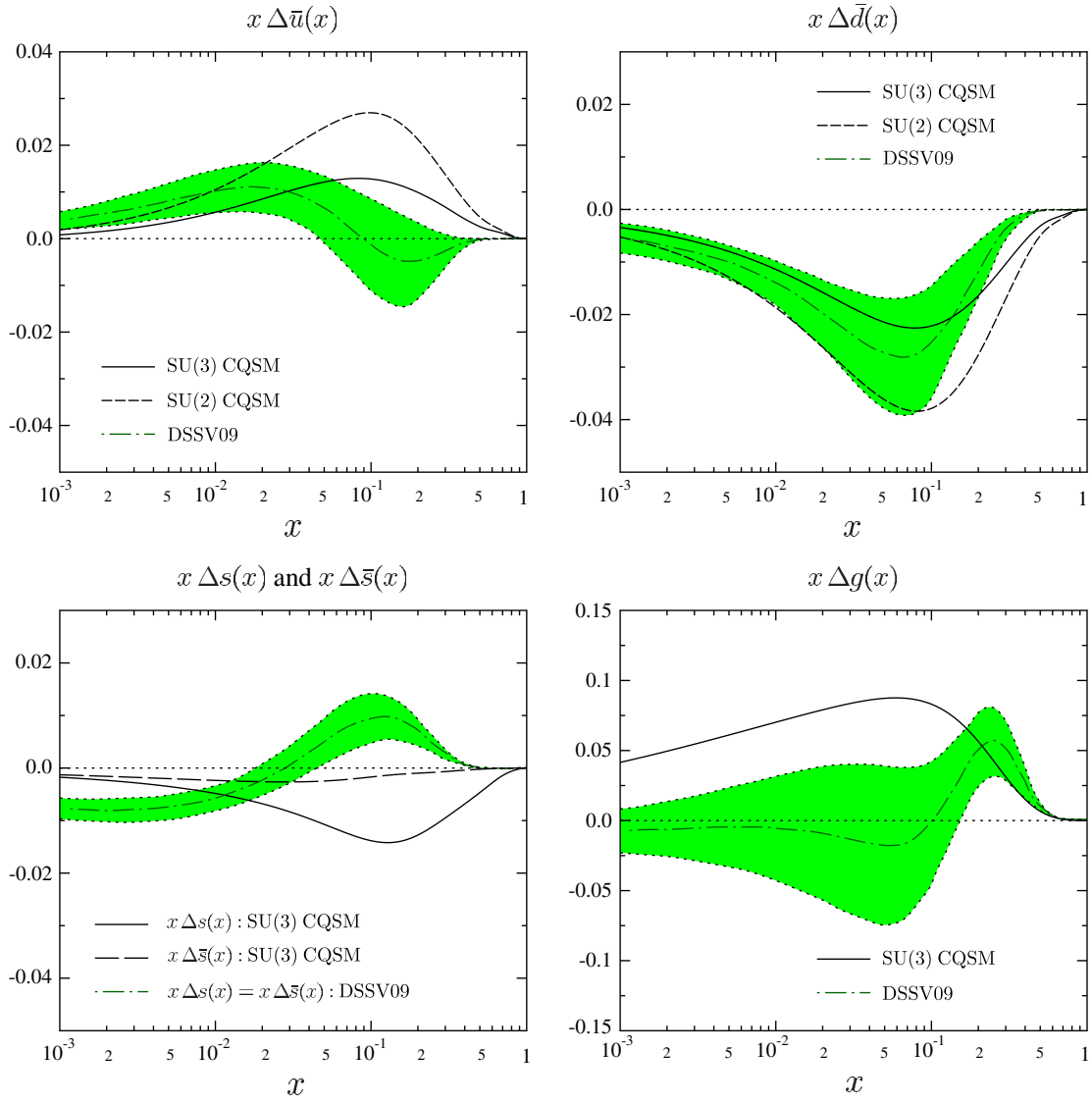

FIG. 15 (color online). The predictions of the SU(3) CQSM for the longitudinally polarized sea-quark distributions $x\bar{u}(x)$, $x\bar{d}(x)$, $x\Delta s(x)$, and $x\bar{s}(x)$, and the polarized gluon distribution $\Delta g(x)$ evolved to $Q^2 = 10$ GeV^2 in comparison with the DSSV09 global fits [105].

as a set in the DSSV09 fits. The model predicts that $x\Delta\bar{u}(x)$ is positive, while $x\Delta\bar{d}(x)$ is negative with sizable magnitude. One confirms that the predictions of the SU(3) CQSM for $x\Delta\bar{u}(x)$ and $x\Delta\bar{d}(x)$ are both consistent at the order-of-magnitude level with the DSSV09 fits. The DSSV central fit for the polarized $\bar{u}$ distribution shows a nodal behavior around $x \sim 0.08$, which is not reproduced by the CQSM. From the theoretical viewpoint, however, such a nodal behavior of the distribution $\Delta\bar{u}(x)$ is difficult to understand. We again suspect that our incomplete understanding of the semi-inclusive processes can be a cause of this unnatural nodal behavior of the global fit. Turning to the strange-quark distributions, the SU(3) CQSM predicts a negative polarization, while the result of the DSSV09 fit is positive in the higher-x range, where the distribution is dominant. However, we have already pointed out that the more recent NNPDF fits give a negative strange-quark polarization [74], which is qualitatively consistent with the prediction of the SU(3) CQSM. Incidentally, in the DSSV analysis, the equality of the polarized strange and antistrange distributions were assumed from the beginning. Very interestingly, according to the SU(3) CQSM, the negative polarization of the strange plus antistrange distribution turns out to mostly come from the strange quark, and the polarization of the antistrange quark is very small. This means that the model predicts a sizable particle-antiparticle asymmetry not only for the unpolarized strange-quark distributions but also for the longitudinally polarized ones. We recall that this feature is also qualitatively consistent with the picture of the kaon cloud model proposed by Signal and Thomas [58], Burkardt and Warr [59], and also by Brodsky and Ma [60]. In fact, the strange sea in the proton is thought to be

generated through the virtual dissociation process of the proton into the Λ and the K^+, i.e., $p \to \Lambda + K^+$. Note the apparent asymmetry of the s quark and $\bar{s}$ quark in this process. The s quark is contained in the spin-1/2 Λ, while the $\bar{s}$ quark is contained in the spin-0 K^+. This naturally explains why the polarization of $\bar{s}$ quark is smaller than that of the s quark.

IV. FLAVOR SU(3) CQSM AND CHARGE-SYMMETRY-VIOLATING PDFs

The effective Lagrangian, which takes account of the CSV, is given as

$$\mathcal{L} = \mathcal{L}_0 + \mathcal{L}_{\rm SB} + \mathcal{L}_{\rm CSV}, \tag{19}$$

where $\mathcal{L}_0$ and $\mathcal{L}_{\rm SB}$ were already given, while the CSV part $\mathcal{L}_{\rm CSV}$ can be written as

$$\mathcal{L} = -\Delta m \bar{\psi} \frac{\lambda_3}{2} \psi, \tag{20}$$

with $\Delta m \equiv m_u - m_d \simeq -4$ MeV. The CSV effects for the PDFs in the nucleon can be investigated by treating this SU(2)-breaking part of the effective Lagrangian as the first-order perturbation. The general method is exactly the same as the one used in the perturbative treatment of the SU(3) symmetry-breaking term $\mathcal{L}_{\rm SB}$. Note however that the mass difference between the u and d quarks is far smaller than that between the strange quark and the u and d quarks. Consequently, the perturbative treatment of the CSV part $\mathcal{L}_{\rm CSV}$ has an even better foundation than that of $\mathcal{L}_{\rm SB}$. Since the necessary formalism was already explained in our previous paper, we do not repeat the detailed derivation here. For completeness, however, we summarize below the final theoretical expressions, which are necessary for the actual calculation.

Within the framework of the SU(3) CQSM, the PDFs for the u, d, and s quarks are represented as linear combinations of three independent functions $q^{(0)}(x)$, $q^{(3)}(x)$, and $q^{(8)}(x)$ as

$$u(x) = \frac{1}{3} q^{(0)}(x) + \frac{1}{2} q^{(3)}(x) + \frac{1}{2\sqrt{3}} q^{(8)}(x), \tag{21}$$

$$d(x) = \frac{1}{3} q^{(0)}(x) - \frac{1}{2} q^{(3)}(x) + \frac{1}{2\sqrt{3}} q^{(8)}(x), \tag{22}$$

$$s(x) = \frac{1}{3} q^{(0)}(x) - \frac{1}{\sqrt{3}} q^{(8)}(x). \tag{23}$$

In the SU(3)-symmetric limit, these three distributions generally consist of the zeroth-order term and the first-order term in the corrective angular velocity Ω of the rotating soliton. (The zeroth-order term corresponds to the mean-field predictions.) They are given as

$$q^{(0)}(x) = \langle 1 \rangle_N \cdot f(x), \tag{24}$$

$$q^{(3)}(x) = \left\langle \frac{D_{38}}{\sqrt{3}} \right\rangle_N \cdot f(x) + \left\langle \sum_{i=1}^{3} \{D_{3i}, R_i\} \right\rangle_N \cdot k_1(x) + \left\langle \sum_{K=4}^{7} \{D_{3K}, R_K\} \right\rangle_N \cdot k_2(x), \tag{25}$$

$$q^{(8)}(x) = \left\langle \frac{D_{88}}{\sqrt{3}} \right\rangle \cdot f(x) + \left\langle \sum_{i=1}^{3} \{D_{8i}, R_i\} \right\rangle_N \cdot k_1(x) + \left\langle \sum_{K=4}^{7} \{D_{8K}, R_K\} \right\rangle_N \cdot k_2(x). \tag{26}$$

The functions $f(x)$, $k_1(x)$, and $k_2(x)$ are defined in Eqs. (33), (76), and (77) of Ref. [53]. (They are all calculable once the solutions of the mean-field equations are given.) Here, the term containing the function $f(x)$ is the zeroth-order term in Ω, while the terms containing the functions $k_1(x)$ and $k_2(x)$ are the first-order terms in Ω. The D_{ab}'s as functions of the collective coordinates ξ_A are the standard Wigner rotation matrices, while R_a is the right-rotation generator [as in the SU(3) Skyrme model]. In the above expressions, $\langle O \rangle_B$ should be understood as an abbreviated notation for the matrix element of a collective operator O between a baryon state B with appropriate quantum numbers, i.e.,

$$\langle O \rangle_B \equiv \int \Psi^{(n)*}_{YTT_3;JJ_3}[\xi_A] O[\xi_A] \Psi^{(n)}_{YTT_3;JJ_3}[\xi_A] d\xi_A. \tag{27}$$

The relevant matrix elements of the collective space operators between the nucleon state appearing in the above expressions are given by Eqs. (186)–(188) of Ref. [53].

There are two types of CSV corrections to the distributions $q^{(0)}(x)$, $q^{(3)}(x)$, and $q^{(8)}(x)$. We can show that the first corrections, which were called the dynamical plus kinematical corrections in Ref. [53] (see also Refs. [106,107]), are given by

$$q^{(0)}(x;\Delta m^{\rm dyn+kin}) = -\frac{2\Delta m I_1}{\sqrt{3}}\langle D_{38}\rangle_N \cdot \tilde{k}_0(x), \tag{28}$$

$$q^{(3)}(x;\Delta m^{\rm dyn+kin}) = -\frac{2\Delta m_s I_1}{3}\langle D_{38}D_{38}\rangle_N \cdot \tilde{k}_0(x) - \Delta m I_1 \left\langle \sum_{i=1}^{3}\{D_{38}, D_{38}\}\right\rangle_N \cdot \left[\tilde{k}_1(x) - \frac{K_1}{I_1}k_1(x)\right] - \Delta m I_2 \left\langle \sum_{i=4}^{7}\{D_{3K}, D_{3K}\}\right\rangle_N \cdot \left[\tilde{k}_2(x) - \frac{K_2}{I_2}k_2(x)\right], \tag{29}$$

$$q^{(8)}(x;\Delta m^{\rm dyn+kin}) = -\frac{2\Delta m I_1}{3}\langle D_{88}D_{88}\rangle_N \cdot \tilde{k}_0(x) - \Delta m I_1 \left\langle \sum_{i=1}^{3}\{D_{8i}, D_{3i}\}\right\rangle_N \cdot \left[\tilde{k}_1(x) - \frac{K_1}{I_1}k_1(x)\right] - \Delta m I_2 \left\langle \sum_{i=4}^{7}\{D_{8K}, D_{3K}\}\right\rangle_N \cdot \left[\tilde{k}_2(x) - \frac{K_2}{I_2}k_2(x)\right]. \tag{30}$$

Here, I_1, I_2, K_1, and K_2 are various moments of inertia of the soliton defined through Eqs. (49)–(52) in Ref. [53]. On the other hand, the functions $\tilde{k}_0(x)$, $\tilde{k}_1(x)$, and $\tilde{k}_2(x)$ are given by Eqs. (142), (155), and (156), respectively, in the same paper [53].

The necessary matrix elements of the collective space operators in the proton state can be easily calculated, and they are shown in Table II. The three matrix elements in the left column take the same values as for the neutron state, whereas the four matrix elements in the right column have the opposite sign of those in the neutron state.

The second correction to the PDFs arises from the mixing of the SU(3) representation by the CSV mass term [53,106,107]. Due to the presence of the CSV mass term, the nucleon state is not a pure SU(3) octet, but it is a linear combination of three SU(3) representations,

$$|N\rangle \simeq |8,N\rangle + d_{\overline{10}}^N|\overline{10},N\rangle + d_{27}^N|27,N\rangle, \tag{31}$$

with the mixing constants

$$d_{\overline{10}}^N = \frac{\sqrt{5}}{15}\left(\alpha' + \frac{1}{2}\gamma'\right)I_2, \tag{32}$$

$$d_{27}^N = -\frac{\sqrt{6}}{75}\left(\alpha' - \frac{1}{6}\gamma'\right)I_2. \tag{33}$$

Here, the constants α' and γ' are given by

$$\alpha' = \left(\frac{\bar{\sigma}}{N_c} - \frac{K_2}{I_2}\right)\frac{\Delta m}{2}, \tag{34}$$

$$\gamma' = -\left(\frac{K_1}{I_1} - \frac{K_2}{I_2}\right)\Delta, \tag{35}$$

with $N_c = 3$ being the number of colors, whereas $\bar{\sigma}$ is defined in Eq. (206) of Ref. [53].

Combining all of the above functions, the CSV corrections to the PDFs can be evaluated in the following manner:

$$\delta u(x) \equiv u^p(x) - d^n(x) = \frac{2}{3}\delta q^{(0)}(x;\Delta m^{\rm dyn+kin}) + [\delta q^{(3)}(x;\Delta m^{\rm dyn+kin}) + \delta q^{(3)}(x;\Delta m^{\rm rep})] + \frac{1}{\sqrt{3}}[\delta q^{(8)}(x;\Delta m^{\rm dyn+kin}) + \delta q^{(8)}(x;\Delta m^{\rm rep})], \tag{36}$$

$$\delta d(x) \equiv d^p(x) - u^n(x) = \frac{2}{3}\delta q^{(0)}(x;\Delta m^{\rm dyn+kin}) - [\delta q^{(3)}(x;\Delta m^{\rm dyn+kin}) + \delta q^{(3)}(x;\Delta m^{\rm rep})] + \frac{1}{\sqrt{3}}[\delta q^{(8)}(x;\Delta m^{\rm dyn+kin}) + \delta q^{(8)}(x;\Delta m^{\rm rep})], \tag{37}$$

$$\delta s(x) \equiv s^p(x) - s^n(x) = \frac{2}{3}\delta q^{(0)}(x;\Delta m^{\rm dyn+kin}) - \frac{2}{\sqrt{3}}[\delta q^{(8)}(x;\Delta m^{\rm dyn+kin}) + \delta q^{(8)}(x;\Delta m^{\rm rep})]. \tag{38}$$

TABLE II. The matrix elements of the relevant collective space operators in the proton state.

—	$\langle \frac{D_{38}}{\sqrt{3}} \rangle_p = \frac{1}{30}$
$\langle D_{38} D_{38} \rangle_p = \frac{1}{15}$	$\langle D_{88} D_{38} \rangle_p = 0$
$\langle \sum_{i=1}^{3} \{D_{3i}, D_{3i}\} \rangle_p = \frac{10}{9}$	$\langle \sum_{i=1}^{3} \{D_{8i}, D_{3i}\} \rangle_p = \frac{2\sqrt{3}}{45}$
$\langle \sum_{K=4}^{7} \{D_{3K}, D_{3K}\} \rangle_p = \frac{34}{45}$	$\langle \sum_{K=1}^{3} \{D_{8K}, D_{3K}\} \rangle_p = -\frac{2\sqrt{3}}{45}$

Now, we show in Fig. 16 the predictions of the SU(3) CQSM for the CSV PDFs evolved to the scale $Q^2 = 10\ \mathrm{GeV}^2$ in comparison with some other theoretical predictions. The solid and long-dashed curves stand for the predictions of the SU(3) CQSM for $x\delta u_V \equiv x[u_V^p(x) - d_V^n(x)]$ and $x\delta d_V \equiv x[d_V^p(x) - u_V^n(x)]$, respectively. The long dash-dotted and dotted curves are the predictions of Rodionov, Thomas, and Londergan based on the bag model with quark-diquark correlations [68]. On the other hand, the short-dashed and short-dash-dotted curves are the predictions of Glück, Jimenez-Delgado, and Reya based on the QED radiative (or splitting) mechanism [70]. (The CSV effects arising from the QED splitting mechanism were also proposed independently by Martin *et al.* [71].)

First, we point out that all the models predict that $\delta u_V(x) < 0$ and $\delta d_V(x) > 0$ at least for the dominant components in the larger-x region. Comparing the predictions of the SU(3) CQSM and those of the bag model, we find that the former are much smaller than the latter. To understand the cause of this difference, it is instructive to compare the basic framework of these models in some detail. In the framework of the CQSM, the mass difference between the u and d quarks is the only origin of the CSV effects in the PDFs. Once the perturbative treatment of this mass difference is accepted, there is no ambiguity in the theoretical treatment. On the other hand, the refined bag-model treatment of Rodionov *et al.* is based on a quite different assumption on the CSV mechanism [68], which was first proposed by Sather [67] and has been used in most investigations of the CSV PDFs in the past. This treatment is critically dependent on the quark-diquark picture for the intermediate states in the DIS amplitudes. To be more concrete, their treatment starts with the parton-model expression for a quark distribution function,

$$q(x) = M_N \sum_X |\langle X|\psi_+(0)|N\rangle|^2 \times \delta(M_N(1-x) - p_X^+), \tag{39}$$

where $\psi_\pm = (1 + \gamma^0\gamma^3)\psi/2$, $|N\rangle$ is the nucleon state, and $|X\rangle$ represents all possible final states, which are obtained from $|N\rangle$ by removing a quark or adding an antiquark. The state $|X\rangle$ is thought to have the following Fock-space expansion: $|X\rangle = 2q, 3q + \bar{q}, 4q + 2\bar{q}, \ldots$. Based on the idea that for large enough x (say, $x \geq 0.2$) the valence quarks dominate, it was postulated that a reasonable estimate of $q(x)$ can be obtained by including only two-quark intermediate states for $|X\rangle$. It was further assumed that this intermediate two-quark state can be approximated by a diquark with definite mass M_D. The validity of both of these assumptions is not absolutely certain. In particular, the latter postulate, i.e., the two-body kinematics in the intermediate state, is a highly nontrivial assumption. We refer to Ref. [108] for a detailed criticism of the framework used for evaluating the CSV effects in PDFs based on the quark-diquark hypothesis.

In any case, a common feature of most calculations based on this quark-diquark picture is that they predict fairly large CSV corrections in PDFs ranging from 2% to 10%, which is much larger than the CSV effects expected from the low-energy CSV phenomena, which are generally known to be less than 1%. In view of this situation, it is important to estimate the size of CSV effects in PDFs without relying upon the quark-diquark picture. So far, there have been only a few such attempts. One is the study by Cao and Signal based on a meson cloud model [108]. In their treatment, hadron mass differences between the isospin multiplets are the only sources of the CSV effects in PDFs. Another independent analysis was carried out by Benesh and Goldman based on a quark model [109]. In their treatment, the effects due to the u-d quark mass difference and the Coulomb interaction of the electrically charged quarks were taken into account. Both of these studies showed that the CSV effects in PDFs are considerably smaller than those obtained based on the quark-diquark picture. The present calculation (based on a totally different theoretical framework) appears to give additional support to this conclusion by Cao and Signal and also by Benesh and Goldman.

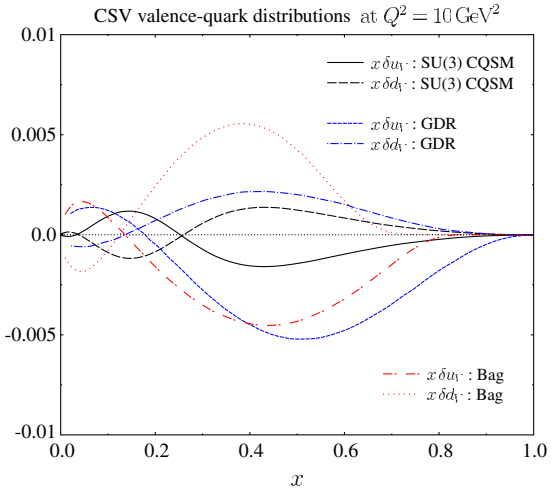

FIG. 16 (color online). The predictions of the SU(3) CQSM for the CSV PDFs $\delta u_V(x)$ and $\delta d_V(X)$ corresponding $Q^2 = 10\,\mathrm{GeV}^2$. Also shown are the bag model predictions by Rodionov-Thomas-Londergan [68], and the predictions based on the QED radiative mechanism due to Glück-Delgado-Reya (GDR) [70].

Since our main purpose in investigating the CSV PDFs is to get a feeling for the relative importance of the CSV effects and the asymmetry of the strange- and antistrange-quark distributions in the resolution of the NuTeV anomaly, we compare these distributions in Fig. 17. Here, the solid curve is the bare prediction of the CQSM for $x[s(x) - \bar{s}(x)]$, while the long-dashed curve is the prediction reduced by a factor of $1/2$. (The latter is our favorable prediction, as explained before.) The dash-dotted curve is the CQSM prediction for the CSV valence distribution $x[\delta u_V(x) - \delta d_V(x)]$ divided by a factor of 2. [To understand why we divide it by 2, compare Eqs. (41) and (42) below.) One sees that the CSV valence-quark distribution is much smaller than the asymmetry of the strange- and antistrange-quark distributions calculated within exactly the same theoretical framework.

As is well known, the main QCD correction to the Paschos-Wolfenstein relation is approximately given by the following formula:

$$R^- \equiv \frac{\sigma^{\nu N}_{\rm NC} - \sigma^{\bar{\nu} N}_{\rm NC}}{\sigma^{\nu N}_{\rm CC} - \sigma^{\bar{\nu} N}_{\rm CC}} = R^-_{\rm PW} + \delta R^-_I + \delta R^-_s, \tag{40}$$

where $\sigma_{\rm NC}$ and $\sigma_{\rm CC}$ respectively stand for the neutrino-nucleon (or antineutrino-nucleon) neutral-current and charged-current cross sections. Here,

$$\delta R^-_I \simeq \left(1 - \frac{7}{3} s^2_W\right) \frac{\delta U_V - \delta D_V}{2(U_V + D_V)}, \tag{41}$$

$$\delta R^-_s \simeq -\left(1 - \frac{7}{3} s^2_W\right) \frac{S^-}{U_V + D_V}, \tag{42}$$

with $s^2_W \equiv \sin^2\theta_W = 0.2227 \pm 0.0004$ and

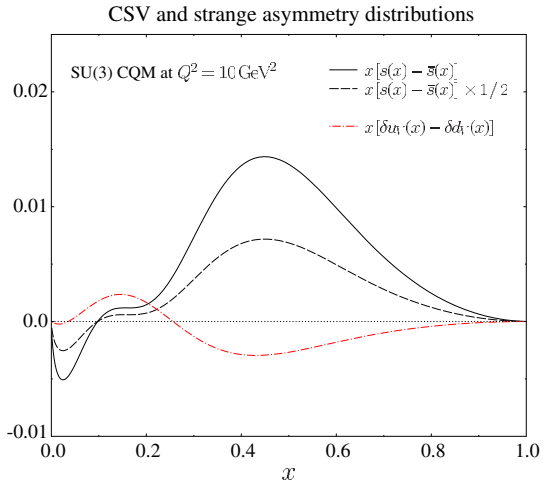

FIG. 17 (color online). The SU(3) CQSM predictions for the CSV valence-quark distribution in comparison with the strange asymmetry distribution.

$$Q_V(Q^2) = \int_0^1 x q_V(x, Q^2) dx, \tag{43}$$

$$\delta Q_V(Q^2) = \int_0^1 x \delta q_V(x, Q^2) dx, \tag{44}$$

$$S^-(Q^2) = \int_0^1 x[s(x, Q^2) - \bar{s}(x, Q^2)] dx. \tag{45}$$

Glück *et al.* [70] as well as the NuTeV Collaboration [56,57] pointed out that the above approximate formula is not accurate enough and proposed a more refined formula to determine the CSV effects on the determination of $\sin\theta_W$. However, since our main interest here is the relative importance of the CSV effects and the particle-antiparticle asymmetry of the strange-quark distribution, we continue to use the above formula. Using the obtained distributions corresponding to the scale $Q^2 = 10\,\mathrm{GeV}^2$, we get the following estimate for the CSV correction from QCD:

$$\Delta s^2_W|_{\rm CSV} \simeq \delta R^-_I|_{\rm QCD} \simeq -0.00035. \tag{46}$$

On the other hand, the correction due to the strange-antistrange asymmetry is given by

$$\Delta s^2_W|_{\rm strange} \simeq \delta R^-_s = -0.00264(-0.00528). \tag{47}$$

Here the number in the parentheses is the bare prediction of the SU(3) CQSM that is not multiplied by a factor of $1/2$. Note that this estimate is consistent at the order-of-magnitude level with the independent estimate by Ding, Xu, and Ma [64], which was $\delta R^-_s \simeq -0.00297$ to -0.00498. Thus the effect of CSV originating from the u-d quark mass difference is an order of magnitude smaller than that of the strange asymmetry. We however recall that there is another mechanism which generates the CSV effects in the quark distributions. It is the QED splitting mechanism proposed by Glück *et al.* and Martin *et al.* The recent estimate by Glück *et al.* gives

$$\Delta s^2_W|_{\rm QED} = \delta R^-_I|_{\rm QED} = -0.002. \tag{48}$$

Since this CSV mechanism is from QED and it is totally independent of the CSV effect of QCD origin, we may add all the above corrections to the Weinberg angle. This gives

$$\begin{aligned} \Delta s^2_W|_{\rm sum} &= \text{QED} + \text{strange} + \text{CSV} \\ &= -0.002 - 0.00264 - 0.00035 \\ &\simeq -0.0050. \end{aligned} \tag{49}$$

This means that the NuTeV measurement of $\sin^2\theta_W = 0.2277(16)$ will be shifted to $\sin^2\theta_W = 0.2227(16)$, which agrees with the standard value 0.2228(4), although we should perform a more careful analysis in light of the approximate nature of the above correction formula.

Nonetheless, our finding here can be summarized as follows. The effect of the particle-antiparticle asymmetry of the strange-quark distribution on the NuTeV anomaly seems to be much larger than the CSV effect in the valence-quark distribution originating from the u-d quark mass difference. However, the CSV effect due to the QED splitting mechanism is an increasing function of the scale [70,71] and its effect on the NuTeV anomaly can have the same order of magnitude as that of the strange asymmetry at the scale of $Q^2 = 10\ \mathrm{GeV}^2$.

Since one of the advantages of the CQSM is that it can give reasonable predictions not only for the quark distributions but also for the antiquark distributions, we think it would be interesting to evaluate the CSV effect in the sea-quark distributions in this model. The solid and long-dashed curves in Fig. 18 represent the CSV light-flavor sea-quark distributions defined by

$$\delta\bar{u}(x) \equiv \bar{u}^p(x) - \bar{d}^n(x), \tag{50}$$

$$\delta\bar{d}(x) \equiv \bar{d}^p(x) - \bar{u}^n(x). \tag{51}$$

Here, the solid and long-dashed curves correspond to the predictions of the SU(3) CQSM, while the dash-dotted and short-dashed curves correspond to the predictions based on the QED splitting mechanism [70]. Very curiously, the predictions of the SU(3) CQSM for $\delta\bar{u}(x)$ and $\delta\bar{d}(x)$ and the corresponding predictions due to the QED splitting mechanism have nearly equal magnitudes but their signs are opposite. This means that, if we add up both contributions, a sizable cancellation occurs, which would indicate that the net CSV effects on the sea-quark distribution would be very small and hard to observe experimentally.

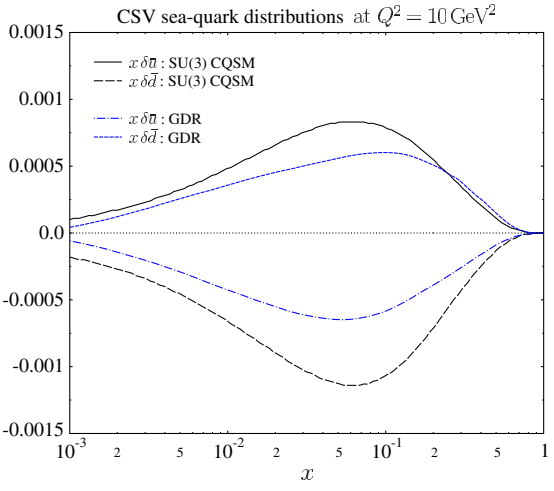

FIG. 18 (color online). The predictions of the SU(3) CQSM for the CSV sea-quark (-antiquark) distributions at $Q^2 = 10\ \mathrm{GeV}^2$ in comparison with the corresponding distributions generated by the QED splitting mechanism due to Glück-Delgado-Reya (GDR) [70].

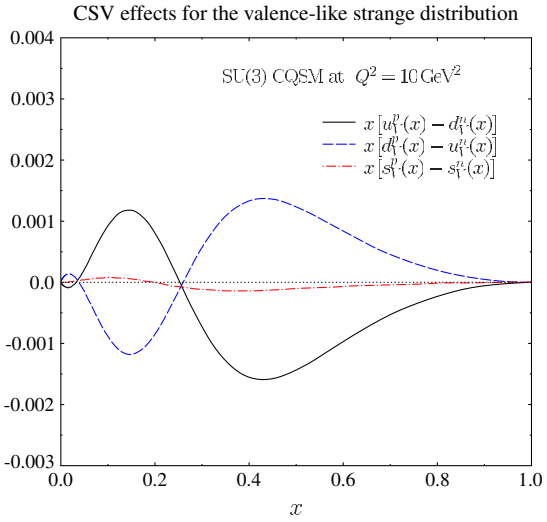

FIG. 19 (color online). The SU(3) CQSM prediction for the CSV effects on the valence-like strange-quark distribution $x[s_V^p(x) - s_V^n(x)]$ with $s_V(x) \equiv s(x) - \bar{s}(x)$ in comparison with the CSV effects on the light-flavor valence-like distributions $x[u_V^p(x) - d_V^n(x)]$ and $x[d_V^p(x) - u_V^n(x)]$.

As a final check, we estimate the CSV effect on the valence-like strange-quark distribution, i.e., $s^-(x) \equiv s(x) - \bar{s}(x)$ in comparison with the CSV effects on the light-flavor valence-quark distribution. The results are shown in Fig. 19, which confirms that the CSV effect on the strange distribution is in fact very small.

V. SUMMARY AND CONCLUSION

To conclude, we have analyzed the unpolarized and longitudinally polarized PDFs in the nucleon within the SU(3) CQSM, which contains only one adjustable parameter, Δm_s, the mass difference between the strange and nonstrange quarks. Through detailed comparisons with the recent global PDF fits by the NNPDF, DSSV, and CTEQ Collaborations (among others), we could confirm that—despite its nearly parameter-free nature—the model reproduces all the qualitative characteristics of the empirically determined PDFs. Besides, it gives unique and nontrivial predictions on the flavor structure of the sea-quark distributions: the flavor asymmetry of the unpolarized sea-quark distributions, $\bar{u}(x) - \bar{d}(x) < 0$, dictated by the famous NMC measurement; the flavor asymmetry of the longitudinally polarized sea-quark distributions, $\Delta\bar{u}(x) > 0$, $\Delta\bar{d}(x) < 0$; the particle-antiparticle asymmetry of the unpolarized strange-quark distribution, $s(x) - \bar{s}(x) \neq 0$; and the particle-antiparticle asymmetry of the longitudinally polarized strange-quark distributions, $\Delta s(x) < 0$, $\Delta\bar{s}(x) \simeq 0$. The success is naturally connected with the fact that the model incorporates the most important feature of QCD in the nonperturbative low-energy domain, i.e., the spontaneous chiral symmetry breaking and the appearance of the associated Goldstone bosons. Still, an important

difference with more familiar meson cloud models should be clearly recognized. As stated above, the CQSM predicts a large isospin asymmetry not only for the unpolarized seas but also for the longitudinally polarized ones. On the other hand, although the meson cloud models nicely explain the flavor asymmetry of the unpolarized sea-quark distributions, they generally predict a very small spin polarization of sea quarks, reflecting the fact that the pion carries no spin and the effects of a heavier meson cloud are suppressed. In light of this important difference, a more unambiguous confirmation of the flavor asymmetry of the longitudinally polarized sea-quark distribution is an urgent task.

We have pointed out that in order for the model predictions to be taken as reliable in a quantitative sense, we need two remedies. First, the information from phenomenological global fits indicates that the gluon carries about 20% of the nucleon momentum fraction even at the low-energy scale corresponding to the CQSM. Naturally, this fact is not properly incorporated in effective quark models like the CQSM. As we have seen, this seems to be a cause of a roughly 20% overestimate of the flavor-singlet combination of the unpolarized PDFs. However, we have also shown that the neglect of the gluon degrees of freedom at the model energy scale is likely to do little harm in the case of the longitudinally polarized PDFs. This is the reason why the success of the model is more salient for the longitudinally polarized PDFs than for the unpolarized PDFs. The second problem is that the SU(3)-symmetric collective quantization (with the subsequent perturbative treatment of the SU(3) symmetry-breaking mass difference between the strange and nonstrange quarks) might tend to overestimate the kaon cloud effects, thereby being in danger of overvaluing the magnitudes of the strange-quark distributions. As the present analysis (especially the detailed comparison with the unbiased NNPDF global fits) strongly indicates, plausible predictions for the strange- and antistrange-quark distributions would correspond to an average of the SU(3) CQSM and the SU(2) CQSM, which means that we can get reliable predictions for the strangeness-related distributions if we multiply the bare predictions of the SU(3) CQSM by a reduction factor of about $1/2$. After this modification to the strange-quark distributions is taken into account, we have good reason to believe that the SU(3) CQSM is already giving reliable predictions with 20–30% accuracy for both the unpolarized and longitudinally polarized PDFs, including the key issues of the present research, i.e., the flavor structure of the sea-quark distribution in the nucleon. We hope that these characteristic predictions reported in the present paper will be tested through more elaborate analyses of the neutrino-induced DIS measurements, the semi-inclusive DIS measurements, the polarized Drell-Yan processes in pp or $p\bar{p}$ collisions, etc., that will be carried out in the near future.

ACKNOWLEDGMENTS

The author would like to thank Y. Nakakoji for his helpful collaboration at the early stage on the investigation of the charge-symmetry-violating parton distributions. He also greatly acknowledges useful discussions with J.-C. Peng and K.-F. Liu at the workshop "Flavor Structure of the Nucleon Sea" held at ECT* in July, 2013.

[1] T. Muta, *Foundations of Quantum Chromodynamics* (World Scientific, Singapore, 1998).
[2] J. Collins, *Foundations of Perturbative QCD* (Cambridge University Press, Cambridge, England, 2011).
[3] M. Anselmino, A. Efremov, and E. Leader, Phys. Rep. **261**, 1 (1995).
[4] B. Lampe and E. Reya, Phys. Rep. **332**, 1 (2000).
[5] P. Jimenez-Delgado, W. Melnitchouk, and F. Owens, J. Phys. G **40**, 093102 (2013).
[6] P. Amaudruz *et al.* (NMC Collaboration), Phys. Rev. Lett. **66**, 2712 (1991).
[7] S. Kumano, Phys. Rep. **303**, 183 (1998).
[8] G. T. Garvey and J.-C. Peng, Prog. Part. Nucl. Phys. **47**, 203 (2001).
[9] J.-C. Peng and J.-W. Qiu, Prog. Part. Nucl. Phys. **76**, 43 (2014).
[10] J. D. Sullivan, Phys. Rev. D **5**, 1732 (1972).
[11] J. J. Aubert *et al.*, Phys. Lett. **123B**, 275 (1983).
[12] S. Kumano, Phys. Rev. D **43**. 3067 (1991).
[13] S. Kumano and J. T. Londergan, Phys. Rev. D **44**, 717 (1991).
[14] M. Wakamatsu, Phys. Rev. D **44**, R2631 (1991).
[15] M. Wakamatsu, Phys. Rev. D **46**, 3762 (1992).
[16] W.-Y. P. Hwang, J. Speth, and G. E. Brown, Z. Phys. A **339**, 383 (1991).
[17] W. Koepf, L. L. Frankfurt, and M. Strikman, Phys. Rev. D **53**, 2586 (1996).
[18] A. Bazarko *et al.* (CCFR Collabotation), Z. Phys. C **65**, 189 (1995).
[19] U.-K. Yang *et al.* (CCFR/NuTeV Collaboration), Phys. Rev. Lett. **86**, 2742 (2001).
[20] V. Barone, C. Pascaud, and F. Zomer, Eur. Phys. J. C **12**, 243 (2000).
[21] R. D. Ball, L. D. Debbio, S. Forte, A. Guffanti, J. I. Latorre, A. Piccione, J. Rojo, and M. Ubiali (NNPDF Collabotation), Nucl. Phys. **B823**, 195 (2009).
[22] A. Alekhin, S. Kulagin, and R. Petti, Phys. Lett. B **675**, 433 (2009).

[23] I. Schienbein, J. Y. Yu, C. Keppel, J. G. Morfín, F. I. Olness, and J. F. Owens, Phys. Rev. D **77**, 054013 (2008).
[24] I. Schienbein, J. Y. Yu, K. Kovařík, C. Keppel, J. G. Morfín, F. I. Olness, and J. F. Owens, Phys. Rev. D **80**, 094004 (2009).
[25] A. Airapetian *et al.* (HERMES Collaboration), Phys. Lett. B **666**, 446 (2008).
[26] A. Airapetian *et al.* (HERMES Collaboration), Phys. Rev. D **71**, 012003 (2005).
[27] K. Ackerstaff *et al.* (HERMES Collaboration), Phys. Lett. B **464**, 123 (1999).
[28] M. Alekseev *et al.* (COMPASS Collaboration), Phys. Lett. B **680**, 217 (2009).
[29] M. Alekseev *et al.* (COMPASS Collaboration), Phys. Lett. B **660**, 458 (2008).
[30] D. de Florian, R. Sassot, and M. Stratmann, Phys. Rev. D **75**, 114010 (2007).
[31] D. de Florian, R. Sassot, and M. Stratmann, Phys. Rev. D **76**, 074033 (2007).
[32] S. Kretzer, Phys. Rev. D **62**, 054001 (2000).
[33] M. Hirai, S. Kumano, T.-H. Nagai, and K. Sudoh, Phys. Rev. D **75**, 094009 (2007).
[34] S. Albino, B. A. Kniehl, and G. Krammer, Nucl. Phys. **B803**, 42 (2008).
[35] R. Seidl *et al.* (Belle Collaboration), Phys. Rev. D **78**, 032011 (2008).
[36] D. I. Diakonov, V. Yu. Petrov, and P. V. Pobylitsa, Nucl. Phys. **B306**, 809 (1988).
[37] M. Wakamatsu and H. Yoshiki, Nucl. Phys. **A524**, 561 (1991).
[38] S. Kahana and G. Ripka, Nucl. Phys. **A429**, 462 (1984).
[39] M. Wakamatsu, Prog. Theor. Phys. Suppl. **109**, 115 (1992).
[40] C. V. Christov, A. Blotz, H.-C. Kim, P. V. Pobylitsa, T. Wakabe, T. Meissner, E. Ruiz Arriola, and K. Goeke, Prog. Part. Nucl. Phys. **37**, 91 (1996).
[41] R. Alkofer, H. Reinhardt, and H. Weigel, Phys. Rep. **265**, 139 (1996).
[42] D. I. Diakonov and V. Yu. Petrov, *At the Frontier of Particle Physics* (World Scientific, Singapore, 2001), Vol. 1.
[43] D. I. Diakonov, V. Yu. Petrov, P. V. Pobylitsa, M. V. Polyakov, and C. Weiss, Nucl. Phys. **B480**, 341 (1996).
[44] D. I. Diakonov, V. Yu. Petrov, P. V. Pobylitsa, M. V. Polyakov, and C. Weiss, Phys. Rev. D **56**, 4069 (1997).
[45] P. V. Pobylitsa, M. V. Polyakov, K. Goeke, T. Watabe, and C. Weiss, Phys. Rev. D **59**, 034024 (1999).
[46] H. Weigel, L. Gamberg, and H. Reinhardt, Mod. Phys. Lett. A **11**, 3021 (1996).
[47] H. Weigel, L. Gamberg, and H. Reinhardt, Phys. Lett. B **399**, 287 (1997).
[48] L. Gamberg, H. Reinhardt, and H. Weigel, Phys. Rev. D **58**, 054014 (1998).
[49] M. Wakamatsu and T. Kubota, Phys. Rev. D **57**, 5755 (1998).
[50] M. Wakamatsu and T. Kubota, Phys. Rev. D **60**, 034020 (1999).
[51] M. Wakamatsu and T. Watabe, Phys. Rev. D **62**, 054009 (2000).
[52] M. Wakamatsu, Phys. Rev. D **67**, 034005 (2003).
[53] M. Wakamatsu, Phys. Rev. D **67**, 034006 (2003).
[54] H. Chen, F.-G. Cao, and A. I. Signal, J. Phys. G **37**, 105006 (2010).
[55] F.-G. Cao and A. I. Signal, Phys. Lett. B **559**, 229 (2003).
[56] G. P. Zeller *et al.* (NuTeV Collaboration), Phys. Rev. Lett. **88**, 091802 (2002).
[57] G. P. Zeller *et al.* (NuTeV Collaboration), Phys. Rev. D **65**, 111103 (2002).
[58] A. I. Signal and A. W. Thomas, Phys. Lett. B **191**, 205 (1987).
[59] M. Burkardt and B. J. Warr, Phys. Rev. D **45**, 958 (1992).
[60] S. J. Brodsky and B.-Q. Ma, Phys. Lett. B **381**, 317 (1996).
[61] Y. Ding and B.-Q. Ma, Phys. Lett. B **590**, 216 (2004).
[62] J. Alwall and G. Ingelman, Phys. Rev. D **70**, 111505 (2004).
[63] M. Wakamatsu, Phys. Rev. D **71**, 057504 (2005).
[64] Y. Ding, R.-G. Xu, and B.-Q. Ma, Phys. Lett. B **607**, 101 (2005).
[65] J. T. Londergan and A. W. Thomas, J. Phys. G **31**, 1151 (2005).
[66] J. T. Londergan, J. C. Peng, and A. W. Thomas, Rev. Mod. Phys. **82**, 2009 (2010).
[67] E. Sather, Phys. Lett. B **274**, 433 (1992).
[68] E. Rodionov, A. W. Thomas, and J. T. Londergan, Mod. Phys. Lett. A **09**, 1799 (1994).
[69] J. T. Londergan and A. W. Thomas, Phys. Lett. B **558**, 132 (2003).
[70] M. Glück, P. Jimenez-Delgado, and E. Reya, Phys. Rev. Lett. **95**, 022002 (2005).
[71] A. D. Martin, R. G. Roberts, W. J. Stirling, and R. S. Thorne, Eur. Phys. J. C **39**, 155 (2005).
[72] R. Horsley, Y. Nakamura, D. Pleiter, P. E. L. Rakow, G. Schierholz, H. Stüben, A. W. Thomas, F. Winter, R. D. Young, and J. M. Zanotti (CSSM and QCDSF/UKQCD Collaborations), Phys. Rev. D **83**, 051501(R) (2011).
[73] R. D. Ball, V. Bertone, F. Cerutti, L. D. Debbio, S. Forte, A. Guffanti, J. I. Latorre, J. Rojo, and M. Ubiali (NNPDF Collaboration), Nucl. Phys. **B855**, 153 (2012).
[74] R. D. Ball, V. Bertone, F. Cerutti, L. D. Debbio, S. Forte, A. Guffanti, J. I. Latorre, J. Rojo, and M. Ubiali (NNPDF Collaboration), Nucl. Phys. **B855**, 153 (2012).
[75] A. Blotz, D. Diakonov, K. Goeke, N. W. Park, V. Petrov, and P. V. Pobylitsa, Nucl. Phys. **A555**, 765 (1993).
[76] E. Witten, Nucl. Phys. **B223**, 422 (1983).
[77] M. A. Nowak, P. O. Mazur, and M. Praszalowicz, Phys. Lett. **147B**, 137 (1984).
[78] E. Guadagnini, Nucl. Phys. **B236**, 35 (1984).
[79] D. I. Diakonov and V. Yu. Petrov, Nucl. Phys. **B272**, 457 (1986).
[80] D. I. Diakonov, Prog. Part. Nucl. Phys. **51**, 173 (2003).
[81] A. D. Martin, R. G. Roberts, W. J. Stirling, and R. S. Thorne, Eur. Phys. J. C **35**, 325 (2004).
[82] A. D. Martin, W. J. Stirling, and R. S. Thorne, Phys. Lett. B **636**, 259 (2006).
[83] P. J. Mulders and S. J. Pollock, Nucl. Phys. **A588**, 876 (1995).
[84] E. Ruiz Arriola, Nucl. Phys. **A641**, 461 (1998).

[85] V. Yu. Petrov, P. V. Pobylitsa, M. V. Polyakov, I. Böring, K. Goeke, and C. Weiss, Phys. Rev. D **57**, 4325 (1998).
[86] H. Yabu and K. Ando, Nucl. Phys. **B301**, 601 (1988).
[87] C. G. Callen, K. Hornbostel, and I. Klebanov, Phys. Lett. B **202**, 269 (1988).
[88] J. P. Blaizot, M. Rho, and N. N. Sccocola, Phys. Lett. B **209**, 27 (1988).
[89] W.-C. Chang and J.-C. Peng, Phys. Lett. B **704**, 197 (2011).
[90] K.-F. Liu, W.-C. Chang, H.-Y. Cheng, and J.-C. Peng, Phys. Rev. Lett. **109**, 252002 (2012).
[91] S. J. Brodsky, P. Hoyer, C. Peterson, and N. Sakai, Phys. Lett. **93B**, 451 (1980).
[92] S. J. Brodsky, C. Peterson, and N. Sakai, Phys. Rev. D **23**, 2745 (1981).
[93] E. Leader, A. V. Sidorov, and D. B. Stamenov, arXiv:1406.4678 [Phys. Rev. D (to be published)].
[94] A. Airapetian *et al.* (HERMES Collaboration), Phys. Rev. D **89**, 097101 (2014).
[95] M. Stolarski, arXiv:1407.3721.
[96] P. M. Nadolsky, H.-L. Lai, Q.-H. Cao, J. Huston, J. Pumplin, D. Stump, W.-K.Tung, and C.-P. Yuan (CTEQ Collaboration), Phys. Rev. D **78**, 013004 (2008).
[97] H. L. Lai, M. Guzzi, J. Huston, Z. Li, P. M. Nadolsky, J. Pumplin, and C. P. Yuan, Phys. Rev. D **82**, 074024 (2010).
[98] W.-C. Chang and J.-C. Peng, Phys. Rev. Lett. **106**, 252002 (2011).
[99] K.-F. Liu and S. J. Dong, Phys. Rev. Lett. **72**, 1790 (1994).
[100] K.-F. Liu, Phys. Rev. D **62**, 074501 (2000).
[101] A. V. Efremov, K. Goeke, and P. V. Pobylitsa, Phys. Lett. B **488**, 182 (2000).
[102] D. de Florian, R. Sassot, M. Stratmann, and W. Vogelsang, Phys. Rev. Lett. **113**, 012001 (2014).
[103] D. de Florian, R. Sassot, M. Stratmann, and W. Vogelsang, Phys. Rev. Lett. **101**, 072001 (2008).
[104] B. Dressler, K. Goeke, M. V. Polyakov, and C. Weiss, Eur. Phys. J. C **14**, 147 (2000)
[105] D. de Florian, R. Sassot, M. Stratmann, and W. Vogelsang, Phys. Rev. D **80**, 034030 (2009).
[106] A. Blotz, M. Praszalowicz, and K. Goeke, Phys. Rev. D **53**, 485 (1996).
[107] M. Wakamatsu and N. Kaya, Prog. Theor. Phys. **95**, 767 (1996).
[108] F.-G. Cao and A. I. Signal, Eur. Phys. J. C **21**, 105 (2001).
[109] C. J. Benesh and T. Goldman, Phys. Rev. C **55**, 441 (1997).